UNIVERSIDAD DE CHILE

FACULTAD DE CIENCIAS FÍSICAS Y MATEMÁTICAS

DEPARTAMENTO DE GEOLOGÍA

NUEVO PROCEDIMIENTO PARA ANALIZAR CRYSTAL SIZE DISTRIBUTIONS Y CÁLCULO DE T Y P_{H2O} EN SISTEMAS MAGMÁTICOS A TRAVÉS DE UN MODELO ACOPLADO DE PARÁMETROS CINÉTICOS DE CRISTALIZACIÓN CON LA COMPOSICIÓN DE PLAGIOCLASA. APLICACIONES EN EL VOLCÁN VILLARRICA (CHILE) Y EN EL VOLCÁN LASSEN PEAK (EEUU)

TESIS PARA OPTAR AL GRADO DE MAGÍSTER

EN CIENCIAS, MENCIÓN GEOLOGÍA

MEMORIA PARA OPTAR AL TÍTULO DE GEÓLOGO

CLAUDIO IGNACIO CONTRERAS HIDALGO

PROFESOR GUÍA:

MIGUEL ÁNGEL PARADA REYES

MIEMBROS DE LA COMISIÓN:

ÁNGELO CASTRUCCIO ÁLVAREZ

FRANCISCO GUTIÉRREZ FERRER

SANTIAGO DE CHILE

2015

NUEVO PROCEDIMIENTO PARA ANALIZAR CRYSTAL SIZE DISTRIBUTIONS Y CÁLCULO DE T Y PH2O EN SISTEMAS MAGMÁTICOS A TRAVÉS DE UN MODELO ACOPLADO DE PARÁMETROS CINÉTICOS DE CRISTALIZACIÓN CON LA COMPOSICIÓN DE PLAGIOCLASA. APLICACIONES EN EL VOLCÁN VILLARRICA (CHILE) Y EN EL VOLCÁN LASSEN PEAK (EEUU)

El presente trabajo presenta un nuevo método para desarrollar *Crystal Size Distributions* (CSD), un tipo de análisis textural cuantitativo que compara la densidad de población de cristales respecto a su tamaño. Basado en la modelación de la curva de distribución acumulada del tamaño de cristales a través de una función error, se obtienen CSD los que permiten calcular tasas de crecimiento y nucleación de distribución gaussiana asimétrica con respecto al tiempo. Este procedimiento fue aplicado en una muestra de la erupción de 1971 del volcán Villarrica entregando el tamaño límite que distingue microlitos de fenocristales y mostrando un fuerte incremento de las tasas de crecimientos y nucleación de cristales en 2 y 8 órdenes de magnitud, respectivamente, producto del ascenso de magma y cristalización en superficie. Este procedimiento también fue aplicado en cuarzo-monzodioritas del Plutón La Gloria, entregando una distribución sigmoidal de la fracción volumétrica de cristales con respecto al tiempo la que puede ser dividida en 3 etapas diferentes: una primera que muestra un muy bajo incrementos de la fracción volumétrica, la cual coincide con el pico de la tasa de crecimiento, una segunda que muestra un alto incremento de la fracción volumétrica, la cual coincide con el pico de la tasa de nucleación y una tercera que muestra una segunda disminución debido al bajo volumen disponible para nuclear nuevos cristales y recrecer antiguos.

A pesar de los aportes que genera este nuevo método, el CSD seguiría siendo insuficiente para identificar distintos procesos magmáticos tales como ascenso de magma respecto a cristalización en superficie o mezcla de magmas, calentamientos o sistemas multireservorios. Es por esto que se acoplan los parámetros cinéticos de cristalización calculados a partir de CSD con la composición de plagioclasas ya que ambos dependen tanto de la temperatura como de la presión de agua. El modelo de acoplamiento es aplicado a la erupción de 1915 del Volcán Lassen Peak. Se registran dos procesos de calentamiento previo a la erupción, el segundo producto de mezcla de magmas dacíticos y andesíticos. Se registran condiciones estables del reservorio dacítico a presión de agua de 200 MPa, 830 °C generando plagioclasas de contenido de anortita alrededor de 0.37 con lo que se infiere una cota mínima de profundidad del reservorio de 7 km. Posterior al calentamiento se registra una etapa de devolatilización a una temperatura estable de 940 °C y el ascenso de magma el cual ocurriría en 18 horas.

Dedicatoria

Este trabajo está dedicado a mi familia, quienes me han acompañado con su energía y paciencia.

A Florencia y Antonia por su alegre presencia y por todo el tiempo que no les dediqué.

A Gabriel y Esteban por distraerme cuando era necesario.

A mis padres, Jeannette, Mario, Ximena y Leonel, quienes construyeron enérgicamente mis estructuras psíquicas, morales, emocionales y sociales: todo raciocinio, forma, adorno, perífrasis y arte en este documento llevan sus créditos. Particularmente, a este último, quien, dolorosamente, no podrá vivir la última etapa de este proceso siendo quien con más orgullo lo hubiera presenciado...

Agradecimientos

Al profesor Miguel Ángel Parada Reyes, profesor guía de esta tesis, por su constante apoyo personal y académico. A los profesores Angelo y Francisco, por su activa participación en este trabajo.

Al compañero Eduardo Morgado Bravo con quien vivimos este proceso en conjunto, discutiendo sobre petrología y volcanología, analizando asuntos de la tesis de alguno de los dos, conversando de política, sociedad o fútbol. También a los compañeros Juan Norambuena, Rayén Gho, María Angélica Contreras, Gabriela Pedreros, Alejandra Salas, Exequiel Varela, Francisco Cáceres, Consuelo Martínez, Paulo Quezada, Paula Araya, Mauricio Valenzuela y Fernanda Álvarez por su directa o indirecta colaboración en este trabajo.

Tabla de contenido

Índice de Tablas

Índice de Ilustraciones

Capítulo 1

Introducción

Fundamentación del problema

Los procesos magmáticos pueden estudiarse mediante análisis de geoquímica de roca total (e.g., Ernst et al., 1988; Murphy et al., 2000), análisis de geoquímica mineral (e.g., Bouvet de Maisonneuve et al., 2012; Bouvet de Maisonneuve et al., 2013), termodinámica numérica (e.g., Lohmar et al., 2012; Ustunisik et al., 2014) o análisis textural cuantitativo (e.g., Shea et al., 2010; Spillar and Dolejs, 2015), entre otros.

El análisis textural cuantitativo puede determinar procesos magmáticos a través de distintos parámetros texturales tales como densidad (e.g., Riker et al., 2009), volumen (e.g., Zieg and Marsh, 2002), morfología (e.g., Moitra et al., 2013) y tamaño (e.g., Marsh, 1998 y referencias dentro de este) tanto de cristales como de vesículas. Basado en el tamaño de los cristales se realiza el método más común de análisis textural cuantitativo: *Crystal Size Distribution* (CSD). El CSD compara el número de cristales de cierto tamaño que existen en una unidad volumétrica (densidad de población de cristales) con su respectivo tamaño.

Matemáticamente, el CSD es calculado a partir de una ecuación de continuidad suponiendo un sistema abierto, cristalización en equilibrio e independencia del tamaño inicial entregando una curva recta de pendiente negativa en un diagrama semi-log (Marsh, 1988). Basado en el valor de la pendiente del CSD se puede obtener la tasa de crecimiento y la duración de la cristalización y basado en la intersección con el eje Y se puede obtener la tasa de nucleación de cristales (Marsh, 1988). Empíricamente, el tamaño de los cristales es calculado a partir de imágenes en 2D convirtiendo los valores de densidad (Wager, 1961) y tamaño (Saltikov, 1967; Higgins, 2000) a cristales en 3D. La conversión de densidad y tamaño se hace basado en una única razón de aspecto arbitraria o calculada (Morgan y Jerram, 2006). Este supuesto es erróneo ya que supone un *undercooling* constante (Lofgren, 1974; Pupier et al., 2008; Shea and Hammer, 2013) y las rocas ígneas presentan una alta dispersión de razones de aspecto (Mock and

Jerram, 2005; Jerram and Higgins, 2007). Una vez transformados los cristales a figuras en 3D, se calcula la curva de distribución acumulada de cristales. La derivada de la distribución acumulada de cristales respecto del largo de los cristales es la densidad de población de cristales (Marsh, 1988). Convencionalmente, la curva de distribución acumulada de cristales es dividida en segmentos usando una distribución logarítmica (Higgins, 2002a). Cada segmento es modelado como una línea recta. En consecuencia, cada intervalo es representado por un punto en un diagrama CSD. Convencionalmente, este gráfico discontinuo es interpolado para forzar la obtención de líneas rectas con pendientes negativas, y así, calcular tasas de crecimiento y nucleación de cristales constantes. Este trabajo pretende entregar una alternativa a la conversión estereológica de cristales y al tratamiento matemático para la obtención de tasas de crecimiento y nucleación de cristales modelando la curva de distribución acumulada de cristales como una función continua y derivable.

Las tasas de crecimiento y nucleación de cristales han sido modeladas en diversos modelos. El modelo de sistema abierto entrega una tasa de crecimiento constante y una tasa de nucleación constantes (Marsh, 1988). El modelo de "*Batch System*", el cual supone un sistema cerrado, supone una tasa de crecimiento constante y una tasa de nucleación de distribución exponencial creciente respecto del tiempo (Marsh, 1998). Finalmente, el modelo de inversión de CSD calcula una tasa de crecimiento de distribución exponencial decreciente y una tasa de nucleación de distribución exponencial creciente respecto del tiempo basado en una curva de distribución sigmoidal de la fracción volumétrica de cristales respecto del tiempo (Spillar and Dolejs, 2013). Ninguno de estos tres modelos presenta una distribución gaussiana asimétrica de las tasas de crecimiento y nucleación de cristales respecto del tiempo o del *undercooling* (Spohn et al, 1988; Hort and Spohn, 1991; Hort, 1997; Couch et al., 2003). Este trabajo pretende calcular las tasas de crecimiento y nucleación de cristales en función del tiempo con una distribución gaussiana asimétrica y un peak de la tasa de nucleación posterior al peak de la tasa de crecimiento basado en el modelamiento de la curva de distribución acumulada de cristales como una función continua y derivable.

Este nuevo procedimiento para analizar CSD es aplicado en una muestra de lava de la erupción de 1971 del Volcán Villarrica y en una muestra de cuarzomonzodiorita del Plutón La Gloria debido al buen registro histórico y geológico de la erupción y al impacto

social y turístico de este complejo volcánico y al registro textural y geocronológico del segundo.

Las tasas de crecimiento y nucleación de cristales y la fracción volumétrica de cristales son función del undercooling o de la tasa de enfriamiento (e.g., Marsh, 1988; Spohn et al., 1988; Maaloe et al., 1989; Cashman, 1993). Paralelamente, la composición de los minerales es función de parámetros termodinámicos tales como la presión, la fugacidad de oxígeno, la presión de agua y la temperatura (e.g., Bowen, 1913; Yoder and Tilley, 1962; Smith, 1972; Tsuchiyama and Takahashi, 1983; Ghiorso and Sack, 1995; Holland and Powell, 2003; Cashman and Blundy, 2013). Esta transitividad hace inherente una relación entre los parámetros cinéticos de cristales con su composición. Sin embargo, estudios que determinan esta relación lo hacen mediante coeficientes de difusión o partición (Allegre et al., 1981; Lasaga, 1982; L'Heureux, 1993; L'Heureux and Fowler, 1996; Gorokhova and Melnik, 2010) y no basados en análisis de CSD. Este trabajo pretende crear una relación entre la tasa de crecimiento de cristales medida a partir de CSD y la composición de plagioclasa.

Desde un enfoque semicuantitativo, el CSD permite determinar más de una etapa magmática basado en la presencia de *kinks* donde cada segmento sería representativo de una etapa diferente. Convencionalmente, estos se infieren en rocas extrusivas como etapas pre- y syn-eruptivas (e.g., Armienti et al., 1994; Pappalardo y Mastrolorenzo, 2010). Sin embargo, no es posible distinguir procesos mecánicos durante la etapa pre-eruptiva tales como acumulación-fraccionamiento (Higgins, 2002b), *coarsening* (Jerram et al., 1996), mezcla de magmas (Higgins, 1996), sistemas multi-reservorios (Armienti et al., 1994; Marsh, 1998) y zonación de reservorios (Zieg and Marsh, 2002); y no es posible distinguir entre ascenso magmático y cristalización en superficie durante la etapa syn-eruptiva. Este trabajo pretende mejorar la capacidad del CSD para determinar etapas magmáticas a través del seguimiento correlativo de la fracción volumétrica de cristales en función del tamaño y del tiempo y la composición de elementos mayores de plagioclasa.

El modelo presentado es aplicado en la erupción de 1915 del Volcán Lassen Peak (California, Estados Unidos) debido a que fue producida por la mezcla incompleta de magmas dacíticos y andesíticos, y se cuenta con el registro textural cuantitativo y composicional de los distintos miembros. Se utilizan los CSDs de plagioclasa calculados

por Salisbury et al., (2008) en 3 de las 4 muestras presentadas, cambiando la regresión lineal en 3 tramos que los autores realizan por regresiones polinómicas de cuarto orden. Las tasas de crecimiento, nucleación y fracción volumétrica de plagioclasas en función del tamaño y del tiempo son calculadas a partir de CSD. Se utiliza la base de datos de composición de núcleos de plagioclasa y de perfiles de plagioclasa presentada por los autores para generar un perfil composicional en función del tamaño de cristal acoplándolo a la fracción volumétrica de plagioclasa calculada en función del tiempo, y así, determinando escenarios magmáticos con una resolución mayor que solo considerando el análisis de CSD.

Objetivos

1. Desarrollar un método para calcular CSD, tal que G, J y φ obtenidos presenten resultados en función del tiempo similares a los calculados como función de la energía de activación (ΔG).

1.1.   Desarrollar un método independiente de la razón de aspecto de los cristales basado en la distribución acumulada de cristales (N) y que trate esta última como una curva continua.

1.2.   Generar una regresión con N tal que n resulte en una curva de pendiente variable que derive en la obtención de un G y J con forma de campana en función del tiempo.

1.3.   Comprobar la aplicabilidad del modelo tanto en sistemas volcánicos como en sistemas intrusivos usando una muestra de la erupción de 1971 del Volcán Villarrica y otra de cuarzomonzodioritas pertenecientes al Plutón La Gloria.

1.4.   Calcular CSD, G, J y φ de plagioclasa para ambos casos.

1.5.   Determinar escenarios de cristalización para ambos casos según inflexiones en los CSDs o en los parámetros cinéticos calculados.

2. Desarrollar un modelo para la determinación de parámetros termodinámicos a través del acoplamiento de tasas cinéticas de plagioclasa calculadas a partir de CSD con su composición.

2.1.　Establecer relaciones entre parámetros cinéticos de cristales y parámetros termodinámicos.

2.2.　Establecer la composición de plagioclasa en función de parámetros termodinámicos.

2.3.　Establecer una relación entre parámetros cinéticos de cristales de plagioclasa y su contenido que derive en la obtención de parámetros termodinámicos.

2.4.　Comprobar la aplicabilidad del modelo en sistemas magmáticos usando CSDs y perfiles composicionales de plagioclasa pertenecientes a la erupción de 1915 del Volcán Lassen Peak.

2.5.　Calcular G, J, φ, la temperatura y la presión de agua en función del tamaño de cristal y del tiempo.

2.6.　Determinar escenarios de cristalización en función del comportamiento de los parámetros termodinámicos.

2.7.　Interpretar procesos petrológicos a partir de los datos calculados de G, J, φ, temperatura y presión de agua.

Hipótesis

1. El primer objetivo no presenta hipótesis al tratarse de un objetivo metodológico.

2. Como el contenido de anortita en plagioclasa y la fracción volumétrica de cristales dependen de la temperatura y de la presión de agua estos últimos parámetros podrían ser calculados a partir de los primeros.

Metodología

Captura de imágenes

Los cortes transparente pulidos obtenidos a partir de las muestras de mano son digitalizados en un scanner de escritorio de películas. Este tipo de scanner, a diferencia del scanner de papel, captura la imagen desde una zona contraria al de la emisión de luz. El corte transparente es inserto en el scanner de películas entre dos polarizadores fotográficos circulares, esto permite generar una imagen similar a la obtenida a través de

un microscopio óptico a nícoles cruzados, pero obteniendo el máximo índice de birrefringencia para cada cristal. Las imágenes son digitalizadas a 4800 ppp (pixel por pulgadas) por lo que cada pixel tiene una longitud de 5.29 μm. Estas imágenes tienen el objetivo de obtener parámetros texturales de cristales de largo mayor a 50 μm (10 pixeles).

Imágenes de electrones retrodispersados (BSEM images) son obtenidas con el equipo FEI Quanta 2.0, perteneciente al Centro de Excelencia de Geotermia de los Andes (CEGA), ubicado en el Departamento de Geología, Facultad de Ciencias Físicas y Matemáticas de la Universidad de Chile, Santiago, Chile. Las condiciones del equipo para la captura de imágenes fueron: Spot Size de 5, 20 keV, 80 μA, con una distancia de trabajo cercana a 10.0 mm y un zoom de 200X o 600X. La imagen es capturada con un tiempo de actualización de frames de 100 μs y a una resolución de 1024 x 768 pixeles. Estas imágenes tienen el objetivo de obtener parámetros texturales de cristales de largo entre 1 μm y 120 μm.

Procesamiento de imágenes

Ambos tipos de imágenes son procesados en el software JMicrovision® (www.jmicrovision.com). Los minerales son marcados a mano, y no a través de selección de intervalos de canales RGB o IHS, porque se disminuye el error analítico de área de cada cristal debido a pixelaje y porque se puede distinguir entre cristales de una misma fase mineral que están en contacto. Desde este programa se exporta una base de datos con parámetros texturales tales como largo, ancho, orientación, área, posición, entre otros.

Softwares para cálculo de CSDs con método convencional

Los datos de largo y ancho de cristales son insertos en la planilla Excel CSDSlice4.0 (Morgan & Jerram, 2006), la que compara el histograma de razones largo:ancho con una base de datos de 703 combinaciones de razones de aspecto en 3 dimensiones. La razón de aspecto con R^2 más alto respecto de la ingresada es escogida como la razón de aspecto de todos los cristales contenidos en la roca.

Para generar CSDs según el método convencional se utiliza el software CSDCorrections1.5 (http://www.uqac.ca/mhiggins/csdcorrections.html) (Higgins, 2000). En este software es necesario ingresar el largo, ancho, orientación, área y posición de todos los cristales; el área total de la imagen sin considerar el área de vesículas y bordes de imagen; la medida del eje mayor de elipse, que es el output que entrega el software JMicrovision; la razón de aspecto calculada con el software CSDSlice, un índice de redondeamiento y un índice de orientación calculado por el mismo CSDCorrections.

Análisis de microsonda electrónica

Perfiles de plagioclasas y olivinos, pares de olivinos – piroxenos para geotermobarometría y puntos para caracterización de óxidos de Cr-Fe-Ti fueron hechos con una microsonda JEOL JXA 8230 ubicada en el Laboratorio de Microscopía Electrónica y Análisis por Rayos X (LAMARX), Facultad de Matemática, Astronomía y Física de la Universidad Nacional de Córdoba, Córdoba, Argentina. En plagioclasas se midió Na, Mg, Al, Ca, K, Fe y Si a 20 µA y 15 keV con un tiempo de análisis de 10 s y 5 s en *background*, el Sr se obtuvo a 20 µA y 15 keV con un tiempo de análisis de 20 s y 10 s en *background*; fenocristales fueron medidos con un *spot size* de 10 µm y microlitos con un sport size de 2 µm y a 10 keV para evitar fuga de Na, Sr y K. En olivinos se midió Al, Mg, Ca, Ni, Si y Fe a 20 µA y 15 keV con un tiempo de análisis de 10 s y 5 s en *background* con un spot size de 10 µm. En piroxenos y en óxidos de Cr-Fe-Ti se midió Al, Mg, Ca, Ni, Si, Fe, Ti, Mn y Cr a 20 µA y 15 keV con un tiempo de análisis de 10 s y 5 s en *background* con un spot size de 10 µm para fenocristales y 2 µm para microcristales.

Perfiles de plagioclasas y olivinos y pares núcleo-borde en ambos minerales fueron hechos con una microsonda JEOL JXA 8200 ubicada en los Laboratorios Analíticos de la Camborne School of Mines (CSM), College of Engineering, Mathematics and Physical Sciences (CEMPS), University of Exeter, Tremough Campus, Cornwall, United Kingdom. En plagioclasas se midió Si, Na, K, Al, Ca, Mg y Ti a 10 µA y 10 keV con un tiempo de análisis de 20 s y 10 s en *background* y un spot size de 5 µm, Fe y Sr se midió a 10 µA y 10 keV con un tiempo de análisis de 30 s y 15 s en *background* y un spot size de 5 µm. Na y K fueron medidos primeros en sus respectivos espectrómetros para evitar sesgo de análisis por fuga de estos elementos. En olivinos se midió Si y Mg con un

tiempo de análisis de 20 s y 10 s en *background*; Fe, Ca, Al, Ti, Cr y Mn con un tiempo de análisis de 30 s y 15 s en *background* y Ni con un tiempo de análisis de 40 s y 20 s en *background*; todos los elementos fueron medidos a 10 µA y 10 keV y un spot size de 5 µm.

Análisis de geoquímica de roca total

Elementos mayores, trazas y tierras raras fueron analizados en el Laboratorio ActLabs (http://www.actlabs.com/page.aspx?menu=40&app=220&cat1=669&tp=2&lk=no). Elementos mayores fueron medidos con un ICP correspondiente al paquete 4Litho, el hierro bivalente (FeO) fue medido directamente mediante titración al 19%, elementos traza y de tierras raras fueron medidos con un ICP-MS correspondiente al paquete 8-REE.

Capítulo 2

State of the art

Numerical basis of the Open System model

From the first work applied in industrial chemistry (Randolph and Larson, 1971), Marsh and Cashman made the first studies of CSD applied to geological processes, focusing firstly on the theory (Marsh, 1988) and secondly applied to lava lake solidification (Cashman and Marsh, 1988). Based on the former work, the number and the growth rate of crystals are related to changes in time, crystal size and volume of the system through a simple continuity equation for crystal phases (Marsh, 1988)

$$\frac{d(Vn)}{dt} + \frac{d(GVn)}{dL} + Qn = 0 \tag{2.1}$$

Where V is the volume of the system, n is the number of crystals, G is the crystal growth rate, t is time, L is the crystal length and Q is the flow. An open system of constant volume is considered; that means the volume does not depend of time or size, but considers inputs and outputs of magma. Considering τ as the ratio between the volume and the influx, the continuity equation is expressed as (Marsh, 1988).

$$\frac{dn}{dt} + \frac{d(Gn)}{dL} + \frac{n}{\tau} = 0 \tag{2.2}$$

The open system model assumes the crystal growth rate independent of the crystal size (e.g, Kirkpatrick et al., 1979; Muncill and Lasaga, 1987; Marsh, 1998), despite some authors consider a size-dependent crystal growth treatment (e.g, Eberl et al., 1998; Eberl et al., 2002). Moreover, a steady state system is considered that implies the crystal number does not depend on time (Marsh, 1988).

$$\frac{dn}{dL} + \frac{n}{G\tau} = 0 \tag{2.3}$$

A general solution for the equation 2.3 is the CSD expression

$$n(L) = n_0 \exp(-SL) \qquad (2.4)$$

Where $n(L)$ is the population density defined as the number of crystals per unit volume and per size interval. Based on the equation 2.4, the population density as a function of crystals is a straight line in a log-normal diagram. In this kind of diagram, the intercept (n_o) is defined as the nucleation density and S is the slope of the curve (Figure 2.1).

The integration of the product between the population density expression and a power of crystal length is defined as moments of CSD. The zero and first moment define the total number of crystals (N_T) and the total length of crystals (L_T) respectively as

$$N_T = \int_0^{\infty} n(L)dL = \frac{n_0}{S} \qquad (2.5)$$

$$L_T = \int_0^{\infty} L \times n(L)dL = \frac{n_0}{S^2} \qquad (2.6)$$

The ratio between L_T and N_T defines the mean crystal length (L_m), as known as the characteristic length. Because of kinetics, L_m can be defined as the product between the characteristic crystal growth rate (G_c) and the characteristic time (t_c) (Figure 2.1)

$$\frac{L_T}{N_T} = \frac{1}{S} = L_M = G_c \times t_c \qquad (2.7)$$

The characteristic crystal nucleation rate (J_c) is defined as the ratio between the number of crystals and time. Introducing length by chain rule, J_c is expressed as (Marsh, 1988) (Figure 2.1)

$$J_c = \frac{\partial n}{\partial t} = \frac{\partial n}{\partial L} \times \frac{\partial L}{\partial t} = n_0 \times G_c \qquad (2.8)$$

The crystal volume fraction (φ) can be defined by the third moment of CSD (Marsh, 1988)

$$\varphi = \sigma \int_0^\infty L^3 \times n(L)dL = \frac{6\sigma n}{S^4} \qquad (2.9)$$

Where σ is a shape factor. Based on equation 2.9, a discrete form is expressed to define φ (Higgins, 2002a)

$$\varphi = \sigma \sum n(L_i) \times L_i^3 \times W_i \qquad (2.10)$$

Where W_i is the width of the interval i.

Stereology

To apply the numerical basis of CSD in igneous rocks it is necessary to count and to measure crystals inside them. Typically, crystals are measured in thin sections, a section of a rock, slabs or outcrops. All these cases give 2D images; hence, textural parameters such as length, width, orientation, etc, correspond to crystal sections and not to complete crystals. The responsible discipline of converting 2D crystal data in 3D crystal data is Stereology. In quantitative textural analysis for igneous rocks, the first work that gives an expression to convert 2D in 3D data is in Wager (1961)

$$n_V(L_{XY}) = n_A(l_{XY})^{1.5} \qquad (2.11)$$

Where n_A is the measured areal crystal population density, l_{XY} is the measured crystal length between lengths of X and Y, n_V is the calculated volumetric crystal population density and L_{XY} is the calculated large axis of crystals between lengths of X and Y. The Wager's expression modifies the measured crystal population density, but not crystal lengths. Other expressions that only modify the crystal population density are found in Underwood (1970) (equation 2.12) and Royet (1991) (equation 2.13)

$$n_V(L_{XY}) = \frac{n_A(l_{XY})^{1.5}}{\varphi} \qquad (2.12)$$

$$n_V(L_{XY}) = \frac{n_A(l_{XY})}{H_{XY}} \qquad (2.13)$$
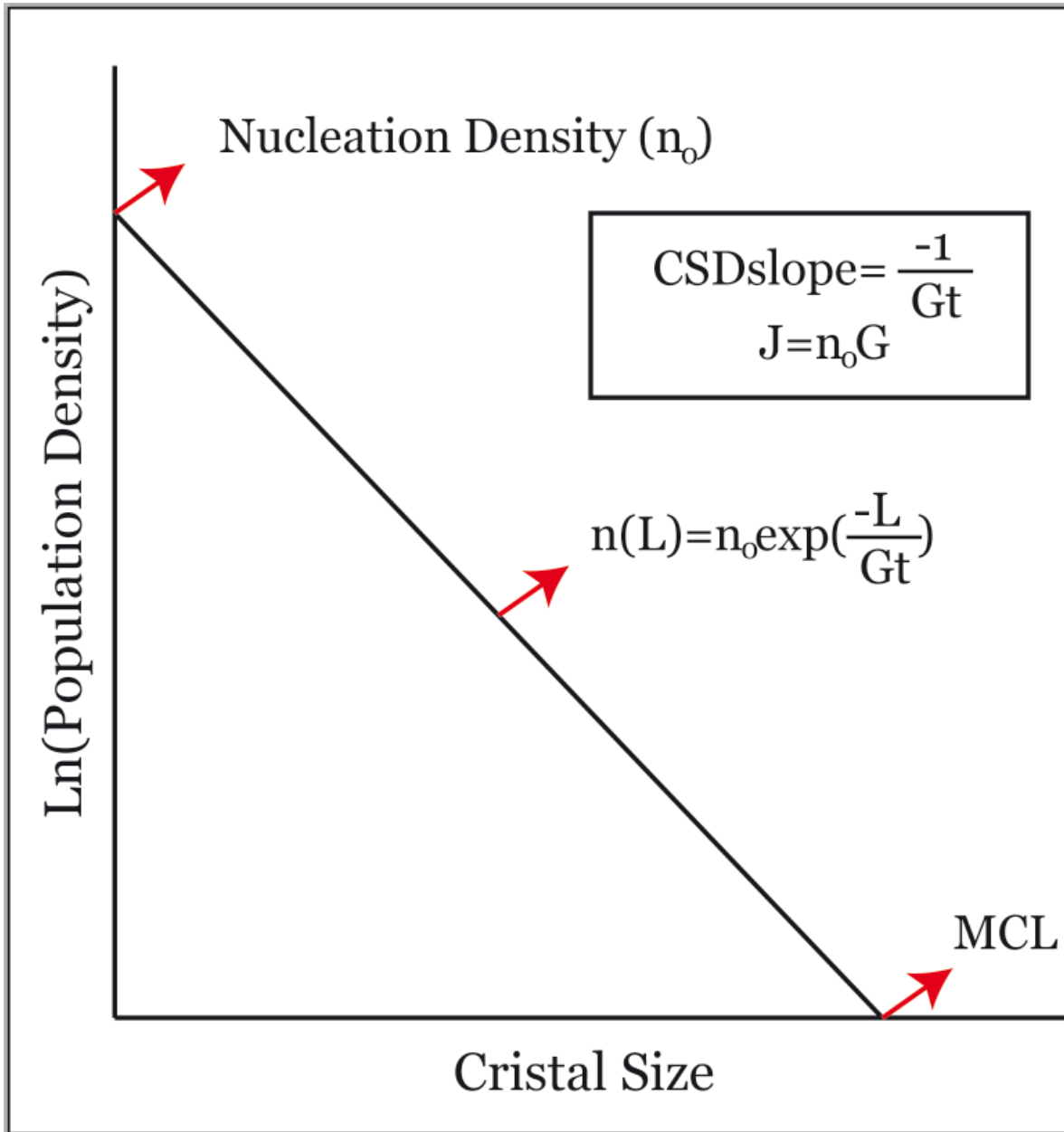
Figure 2. 1: A conventional example of a Crystal Size Distribution (CSD). This diagram compares the population density of crystals versus its crystal size. In a log-normal diagram appears as a perfect straight line based on the Marsh's expression (1988). The slope of this straight line is the inverse of the product between the crystal growth rate (*G*) and the residence time (*τ*). The y-axis intercept defines the nucleation density. The product of the nucleation density and the crystal growth rate defines the crystal nucleation rate (*J*). The crystal growth rate and the crystal nucleation rate are assumed constant by this method. The conventional method does not consider the maximum crystal length (*MCL*).

Where φ is the crystal volume fraction and H_{XY} is the mean projected height between lengths of *X* and *Y*. The last methods do not convert the 2D length in 3D large axis supposing that section cuts all crystals in their center. Alternative methods consider the

cut-section effect measuring the probability of a crystal of being represented in a size interval of lower size due to cuts in crystal corners (Saltikov, 1967; Sahagian and Proussevitch, 1998; Higgins, 2000). These methods suppose a unique and known crystal aspect ratio (size) for all crystals inside a rock and the use of a logarithmical segmentation of the crystal size axis. The expression that defines the calculated volumetric crystal population density in these methods is

$$n_V(L_i) = \frac{n_A(l_i) - \sum_{j=1}^{i-1} n_V(L_j) P_{ji} H_j}{P_{ii} H_i} \tag{2.14}$$

Where $i \in [1...N]$ refers to the crystal size interval (considering the size interval 1 representing the maximum size) and P_{ji} is the probability that a crystal with a true size in interval j will have an intersection that falls in the interval i. Note that these methods use the 3D crystal large axis and not the 2D measured crystal length. The Saltikov's method and the Higgins's method only vary in two aspects: the different conception of the maximum size interval and the calculation of H.

The crystal aspect ratio can be assumed, directly measured or calculated. To calculate it, Higgins (2000) shows that in parallelepipeds the ratio between length (l) and width (w) of 2D images is very similar to the ratio between the small and intermediate axis. The large axis is calculated from the skewness of the the w/l distributions. A complete w/l distribution database is presented by Morgan and Jerram (2006) to compare measured crystal lengths and widths with the database to obtain the crystal aspect ratio.

The use of a unique crystal aspect ratio for a whole igneous rock is naturally controversial. The crystal aspect ratio is a function of the undercooling (the difference between the liquidus temperature and the crystallization temperature) (Lofgren, 1974), as well as the kind of crystallization (homogeneous or heterogeneous) is a function of the undercooling rate (Shea and Hammer, 2013) (Figure 2.2); hence, to assume a unique crystal aspect ratio is to assume the same crystallization temperature history for all crystals. Moreover, direct measurements of crystal aspect ratio through X-ray tomography on feldspars and quartz in natural systems show a strong scattering of the crystal aspect ratios (Mock and Jerram, 2005; Jerram and Higgins, 2007) (Figure 2.3).
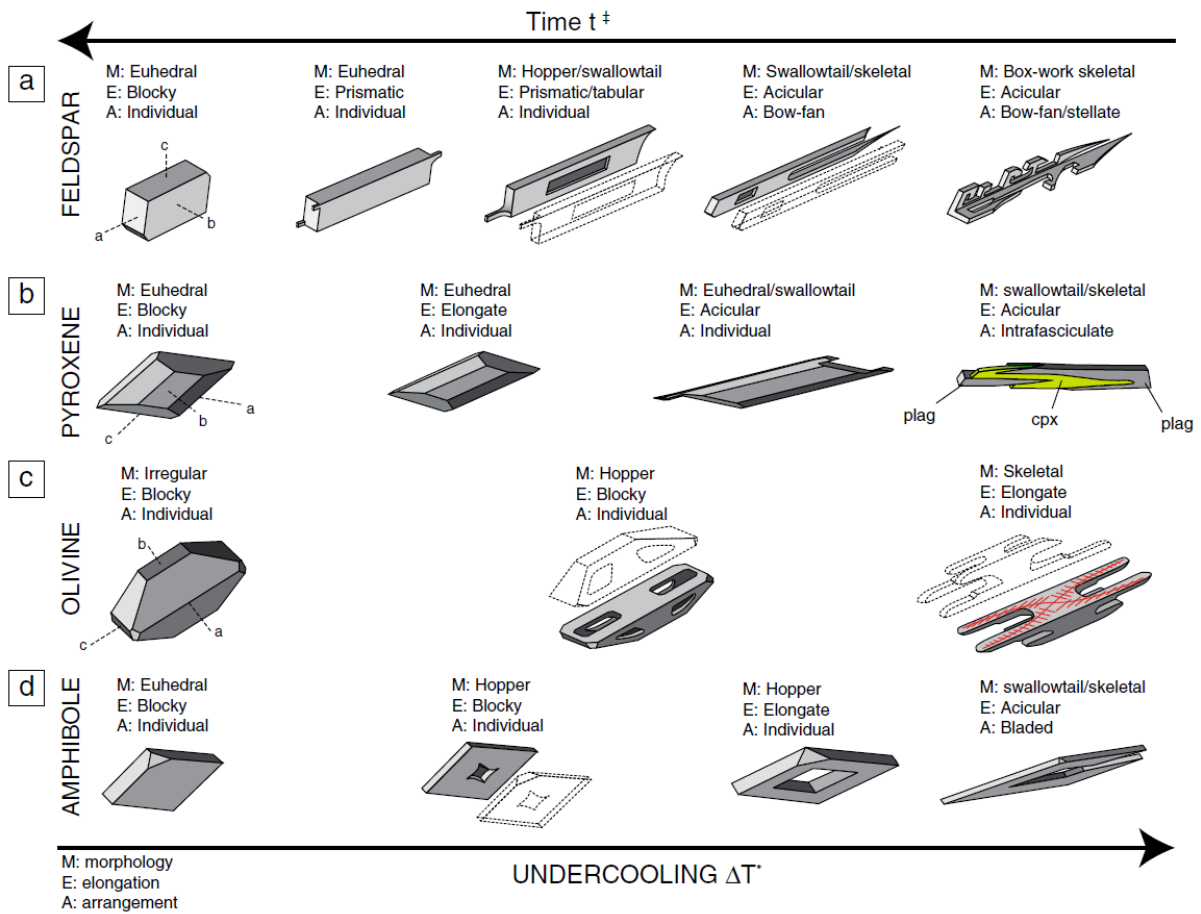
Figure 2. 2: Summary of crystal shapes formed in a hydrous magma as a function of crystallization time and undercooling. The morphology is a function of duration of crystallization and of the undercooling: it varies from euhedral to skeletal with increasing undercooling. The elongation is higher with an increasing undercooling. The terminology is the same used in Lofgren (1974). Extracted from Shea and Hammer (2013).
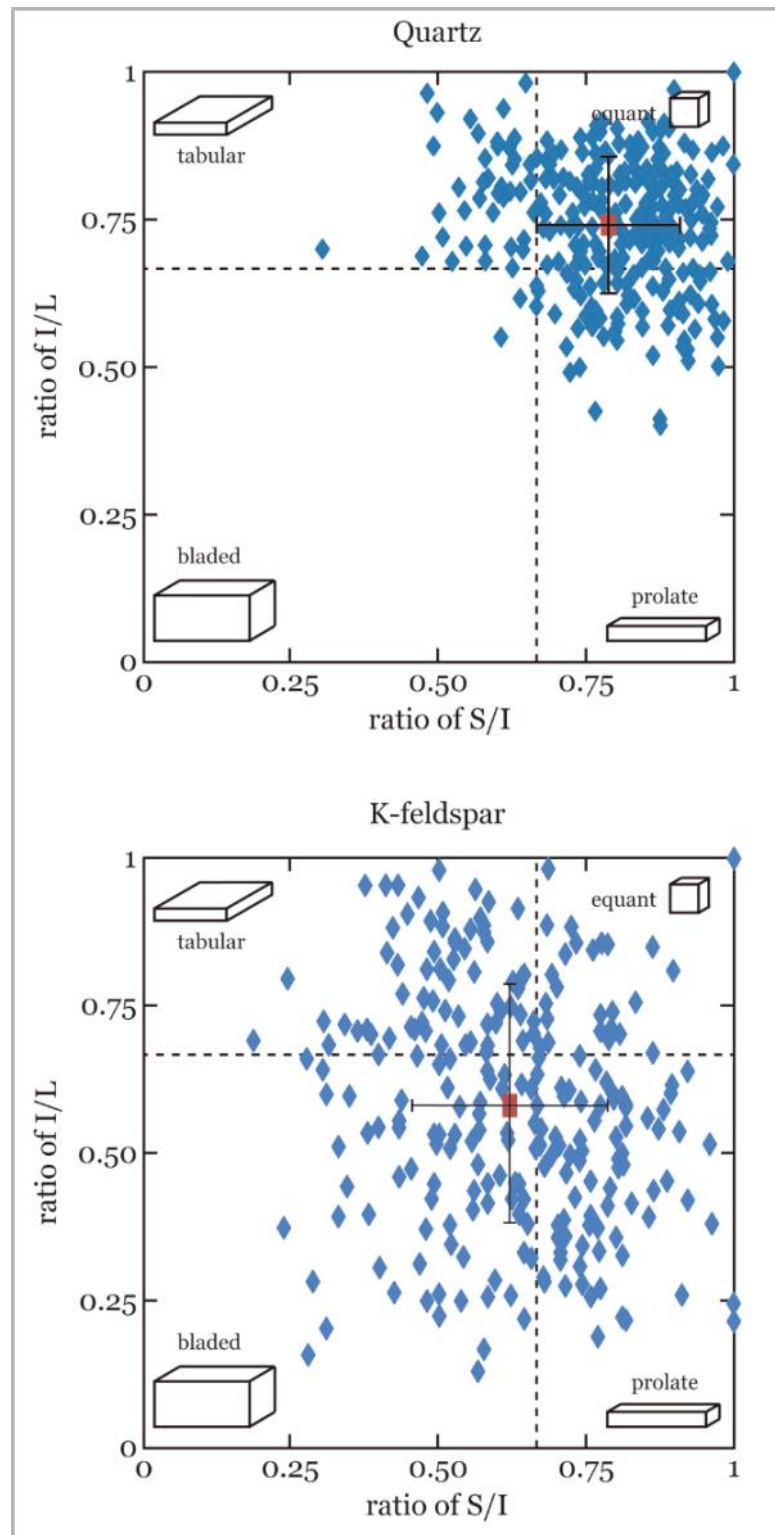
Figure 2. 3: Crystal aspect ratio of k-felspars and quartz from the Late Paleozoic Halle Volcanic Complex. The measured 3D mean aspect ratio in k-feldspar is 1:1.6:2.8 with a small/intermediate axis ratio error of 26.7% and a small/large axis ratio error of 41.1%. The measured 3D mean aspect ratio in quartz is 1:1.3:1.7 with a small/intermediate axis ratio error of 15.6% and a small/large axis ratio error of 20.7%. Modified from Mock and Jerram, 2005 and Jerram and Higgins, 2007.

Other models for CSD calculation

There are some alternatives of the Open System model to analyze CSDs. For example, considering the crystal growth rate dependent on the initial crystal size (e.g., Marsh, 1988; Eberl et al., 1998; Eberl et al., 2002), but this option had not a great impact. The batch system model proposes a time-dependent exponential nucleation and a constant growth of crystals (Marsh, 1998). The resulted CSD is a concave curve with a maximum population density close to the intercept. With a crystal volume fraction lower than 0.5, CSDs modeled by the batch system model are very similar to modeled by the open system model (Figure 2.4). This model does not use the measured maximum crystal length.
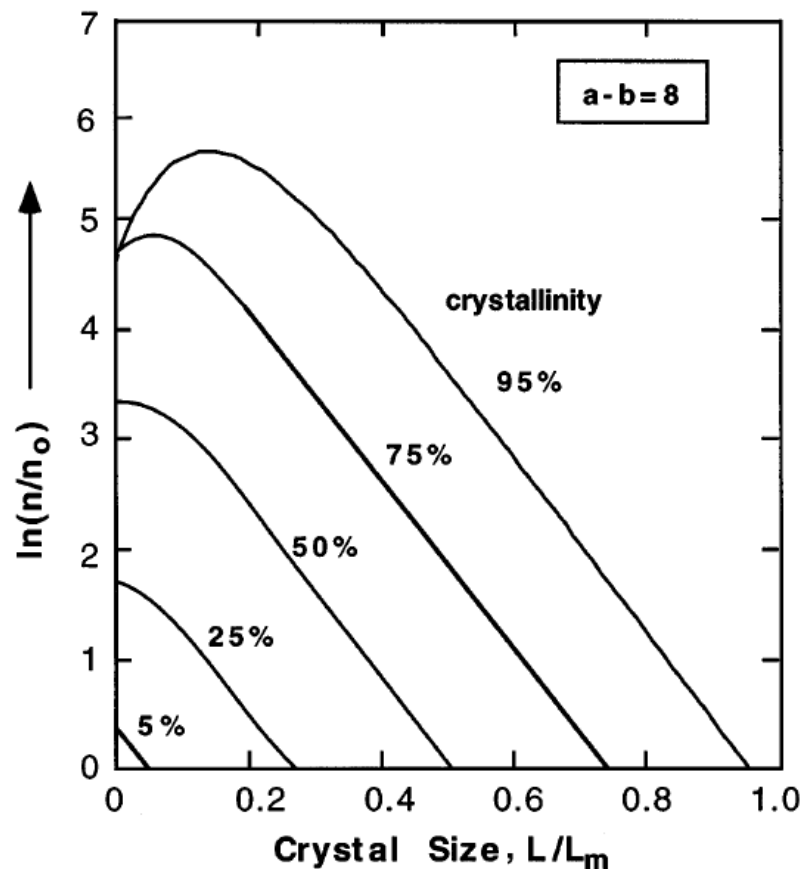
Figure 2. 4: Modeled CSD based on the Match System model (Marsh, 1998). The x-axis is the crystal size normalized by the maximum crystal length for a crystal volume fraction of 1 and the y-axis is the crystal population density normalized by the population density of the maximum crystal length. CSDs are concave curves with a peak close to smallest sizes. The crystal population density increases with an increasing crystallinity. For a crystallinity lower than 50%, CSDs are very similar to CSDs obtained from the Open System model. Extracted from Marsh (1998).

In the current decade, models of inversion of the CSD have been presented (e.g., Melnik et al., 2011; Spillar and Dolejs, 2013). These models are based on the Open System model, but considering the maximum crystal length in spite of the characteristic length. The inversion model calculates kinetic parameters as functions of the time, which advances leftward in the CSD diagram. To consider variations into the CSD slope and the crystal population density, the inversion model parameterizes the crystal size axis in several small segments (Figure 2.4). Inputs to calculate kinetic parameters based on this model are the CSD and crystal volume fraction function. This parameter can be modeled using a sigmoidal expression

$$\varphi(t) = 1 - \exp(-a\pi t^4) \tag{2.15}$$

Where a is a positive constant. The equation 2.15 is consistent with the conventional crystal volume fraction expression as a function of time, crystal growth rate (G) and crystal nucleation rate (J) (Avrami, 1939; Avrami, 1940; Kirkpatrick, 1976).

$$\varphi(t) = 1 - \exp\left\{-\sigma \int_0^t J(\tau)\left[\int_\tau^t G(\tau')\partial\tau'\right]^3 \partial\tau\right\} \tag{2.16}$$

Because of the discretization of the crystal size axis, Spillar and Dolejs (2013) redefine the equation 2.16 in a sum-discrete expression

$$\varphi_{i-1} = 1 - \exp\left(\frac{\sigma}{4}\sum_{j=i}^N \frac{J_j}{G_j}\left\{\left[\sum_{k=i}^{j-1} G_k(t_{k-1} - t_k)\right]^4\right.\right.$$
$$\left.\left. - \left[\sum_{k=i}^{j-1} G_k(t_{k-1} - t_k) + G_j(t_{j-1} - t_j)\right]^4\right\}\right) \tag{2.17}$$

Based on the sigmoidal crystal volume fraction function, the calculated G and J are decreasing and increasing exponential function according to the time respectively.
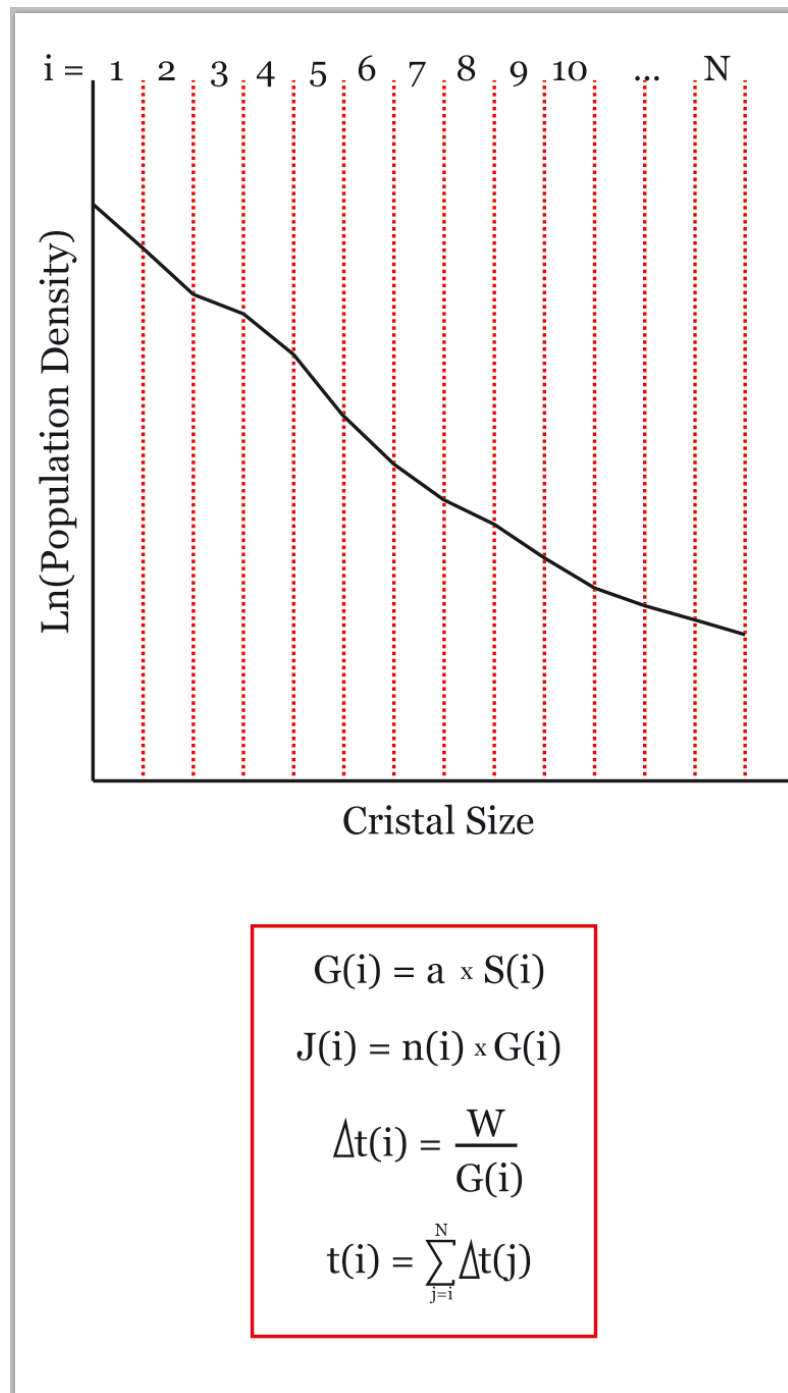
Figure 2. 5: Parameterization of the crystal size axis in the inversion model. The CSD x-axis is parameterized in several segments. This change allows consider soft changes in CSD parameters. Every segment has a representative and constant *G* and *J*. In this case, to calculate *J* is considered the population density of the segment and not the final nucleation density because the population density was the nucleation density when this segment was formed. The duration of crystallization can be calculated as the ratio between the width of the segment and its crystal growth rate. The total duration of crystallization is the cumulative sum from the maximum crystal length to this point.

Crystal kinetic rates as functions of thermodynamic parameters

A lot of works have been focused on the crystal kinetic rate – thermodynamic parameter relationships regardless of the use of quantitative textural analysis. From a more theoretical focus, the crystal nucleation rate (J) is expressed as a function of the temperature (T), the activation energy for the formation of a stable nucleus (ΔG_c) and the activation energy for the diffusion (ΔG_t)

$$J(T) = J_0 \times \exp\left(-\frac{\Delta G_c + \Delta G_t}{RT}\right) \qquad (2.18)$$

Where J_o is a constant and R is the universal gas constant. From the same perspective, the crystal growth rate (G) is expressed as a function of the temperature (T), the activation energy for the diffusion (ΔG_t), the liquidus temperature (T_l) and the difference in free enthalpy between the melt and the crystalline phase (ΔH_v)

$$G(T) = G_0 \times \left[1 - \exp\left(\frac{\Delta H_v(T_l - T)}{RTT_l}\right)\right] \times \exp\left(-\frac{\Delta G_t}{RT}\right) \qquad (2.19)$$

Where G_o is a constant. After of some algebraic operations, as the crystal nucleation rate as the crystal growth rate are expressed as functions of T and T_l (to check previous steps and the final expression, see Spohn et al., 1988). Both crystal kinetic rates have bell-shaped curves with respect to undercooling. The crystal growth rate peak occurs with lower undercooling than the crystal nucleation rate peak (e.g., Spohn et al., 1988; Hort and Spohn, 1991; Hort, 1997) (Figure 2.6). Subsequent experimental works with mafic magmas have obtained similar results in different phases for simple-step and multiple-step experiments (Couch et al., 2003; Shea and Hammer, 2013).

Other perspective expresses both kinetic rates as a function of a power of undercooling (e.g., Marsh, 1988; Maaloe et al., 1989) or of a power of cooling rate (Cashman, 1993; Higgins, 2006).

The crystal volume fraction (φ) has also been expressed as a function of thermodynamic parameters. From a thermal continuity equation, φ is related with latent heat of crystallization obtaining sigmoidal curves with regard to the time (Kirkpatrick,

1976; Blundy et al., 2006). In petrological models, φ has been expressed as a function of T, T_l and the solidus temperature (T_s) following an almost straight curve (e.g., Marsh, 1981; Hort, 1997) described as

$$\varphi(T) = \frac{1}{2}\left[1 + \cos\left(\frac{T - T_s}{T_l - T_s}\pi\right)\right]$$

(2. 20)

Or a third-order polynomial expression (Cashman and Blundy, 2013).
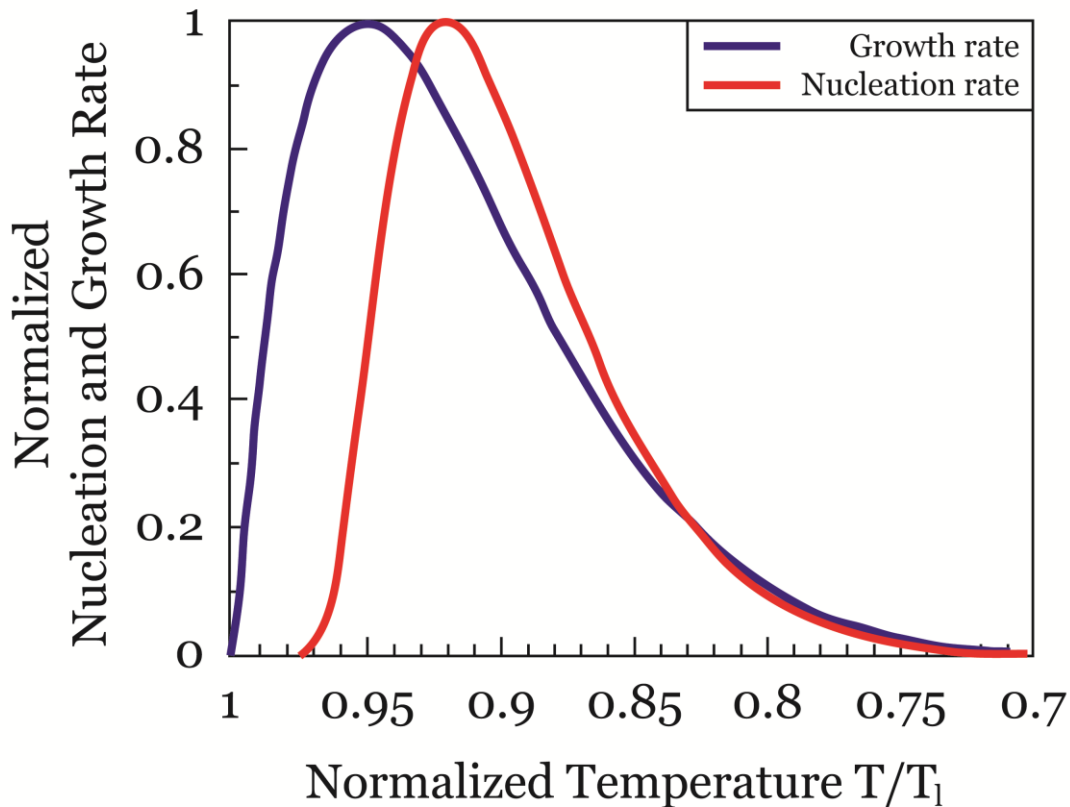
Figure 2. 6: Normalized growth and nucleation rates with respect to temperature-liquidus temperature ratio. Both crystal kinetic rates have bell-shaped curves with respect to temperature, the crystal growth peak occurs with higher temperature than the crystal nucleation rate. Modified from Hort (1997).

Plagioclase composition from a kinetics focus

One of the first works that relates crystal growth rate to the temperature and to plagioclase composition was Kirkpatrick et al.,'s (1979). In this work, plagioclase crystals were obtained from synthetic solutions inside the Anorthite-Albite system. Using An_{100}-Ab_0, An_{75}-Ab_{25}, An_{50}-Ab_{50} and An_{20}-Ab_{80} solutions and changing temperature from 1600

to 900 ºC, crystal growth rates were obtained (Figure 2.7). These results were numerically modeled based on, among other parameters, diffusion and partition coefficients (Lasaga, 1982). Calculated crystal growth rate are not comparable with measured empirically rates because of the use of a single-phase system. Other studies use diffusion coefficients assuming a linear relationship between the temperature and the duration of crystallization or between the temperature and the crystal volume fraction (Allegre et al., 1981; Gorokhova and Melnik, 2010), or using partition coefficients focusing on plagioclase oscillatory zoning in isothermal systems (L'Heureux, 1993; L'Heureux and Fowler, 1996). A few of works relate both parameters through CSDs doing a match between a volumetric parameter based on CSD calculations and a mean plagioclase composition from several igneous bodies (Zieg and Marsh, 2002) or analyzing qualitatively the CSD diagram with the evolution of plagioclase composition (Salisbury et al., 2008).
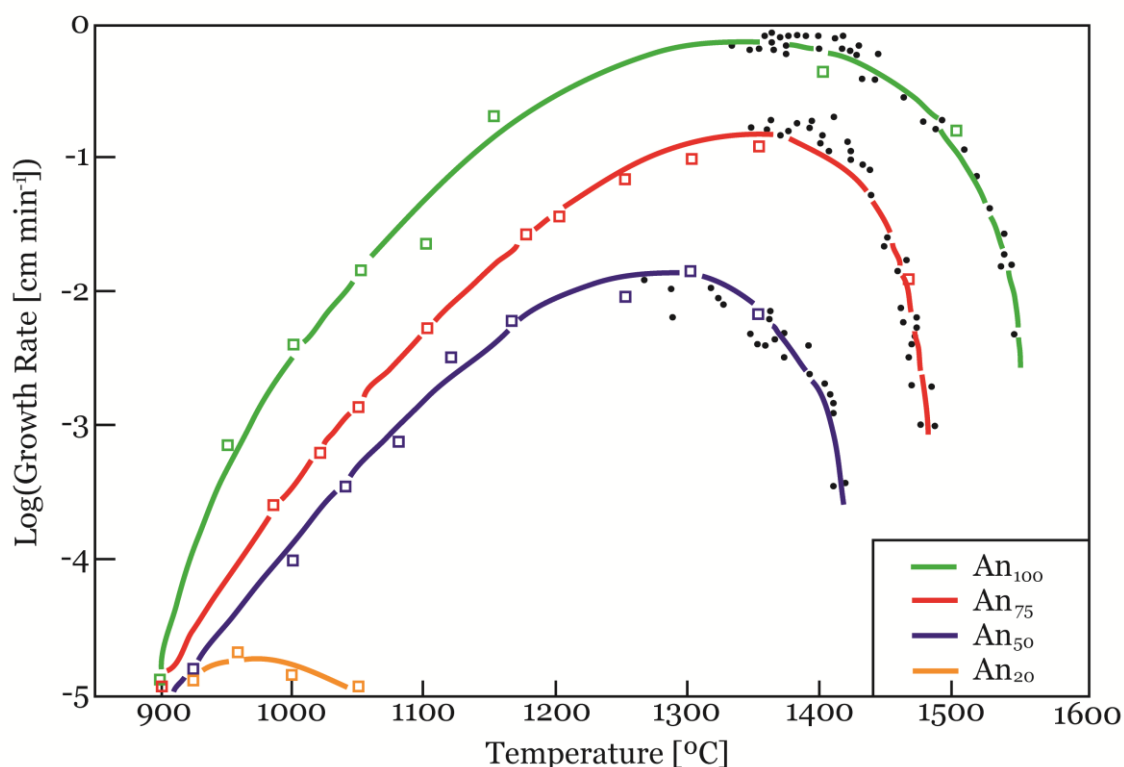
Figure 2. 7: Logarithm of crystal growth rate as a function of temperature for An100-Ab0, An75-Ab25, An50-Ab50 and An20-Ab80 solutions. Small dots are heating stage data. Larger symbols are from quenched samples. According to Kirkpatrick, plagioclase growth rate is higher with increasing anorthite content. For all experiments, the plagioclase growth rate increases from the liquidus temperature, it reaches a peak and later it decreases. Modified from Kirkpatrick et al. (1979).

Crystal Size Distributions applied on volcanoes

The first applied CSD study on volcanoes was in the Makaopuhi Lava Lake (Hawaii) (Cashman and Marsh, 1988), where CSD numerical basis are applied to obtain an exponential relationship between crystal growth rate and cooling rates. The same exponential relationship is exposed as a summary in Cashman (1993) and Higgins (2006). The cooling of magma system affects to other subsurface processes such as magma ascent and surface crystallization. The related textures to these stages are seen in Nanolites and Microlites. Nanolites represent the last portion of magma cooled on surface. Using CSD analysis is possible to describe the evolution of crystallization (Sharp et al., 1996) or to distinguish the beginning of crystallization of different phases (Mujin and Nakamura, 2014). Microlites represent the first stage of crystallization on surface and crystallization during magma ascent. CSD analysis has been used to constraint the evolution of crystallization during the advance of a lava flow (e.g., Crisp et al., 1994; Riker et al., 2009), or to determine different stages of magma ascent (e.g., Preece et al., 2013) or to interpret shallow processes related to cooling (Cashman, 1992) or degassing (Hammer et al., 1999).

Most of the CSD studies focus on petrological processes inside magma reservoirs. Kinks on CSDs could represent the limit between pre-eruptive processes and syn-eruptive processes (e.g., Mastrolorenzo and Pappalardo, 2006; Pappalardo and Mastrolorenzo, 2010) or multi-reservoir systems (Armienti et al., 1994; Marsh, 1998; Armienti et al., 2007). Curvatures on CSD could represent mechanical processes inside magma reservoirs: lower values of population density for smallest sizes than higher sizes imply a digestion of smallest crystals to form regrowth rims in higher crystals, this process is called coarsening (Jerram et al., 1996; Higgins and Roberge, 2003); fractionation-accumulation process is inferred if CSD diagrams are concave or convex (Marsh, 1988; Higgins, 2002b); Magma mixing is inferred if CSDs present kinks with curved segments (Higgins, 1996) or a fanning pattern of a CSD set represents a control by crystal growth rate or residence time because of different cooling regimes (Zieg and Marsh, 2002; Higgins, 2002a).

Capítulo 3

Kinetic parameters and duration of melt crystallization from a new CSD approach

Manuscrito para ser sometido en la revista American Mineralogist

Abstract

Crystal Size Distribution (CSD) is applied in igneous rocks to obtain crystal kinetic parameters such as the crystal growth rate, the crystal nucleation rate and the volume fraction of crystals as functions of the crystal size and the time. The crystal size is usually obtained from measured textural parameters considering a unique crystal aspect ratio regardless of the crystal length, but the morphology of crystals depends on the undercooling and on the cooling rate. The population density of crystals is the differential of the cumulative distribution of crystal lengths function, that is usually discretized using logarithmical distribution with an arbitrary number of bins per decade to obtain CSDs, but the cumulative distribution is a continuous function then no discretization is needed. The discretization of the crystal axis biases the nucleation density, the maximum crystal length and positions of kinks. Consequently, calculated duration of crystallization and the crystal growth rate strongly depend on the number of bins per decade. Here we propose a new procedure to calculate CSD based on the modeling of the cumulative distribution of the crystal lengths function through an error function. Calculated crystal growth rates and crystal nucleation rates have asymmetrical gaussian distributions with regard to the time, where the peak of the former is previous to the peak of the latter and both crystal rates presents an instantaneous increase just previous to an eruption. Calculated volume fraction of crystals has a sigmoidal curve with regard to the time revealing three ideal magmatic stages. This model can be applied both in plutonic and extrusive igneous systems.

Introduction

Crystal Size Distribution (CSD) is a quantitative textural analysis applied in igneous and metamorphic rocks that compares the number of crystals per unit of volume per crystal size, as known as the population density of crystals (n), with its crystal size (L) (Marsh, 1988) in a log-normal diagram. CSD has commonly been used to obtain crystal kinetic parameters such as growth rate (G), nucleation rate (J) or volume fraction (φ) (e.g., Cashman and Marsh, 1988; Cashman, 1993; Crisp et al., 1994; Higgins and Roberge, 2003; Salisbury et al., 2008; Vinet and Higgins, 2010; Spillar and Dolejs, 2013) or to define different magmatic stages (e.g., Armienti et al., 1994; Marsh, 1998; Mastrolorenzo and Pappalardo, 2006; Armienti et al., 2007; Pappalardo and Mastrolorenzo, 2010).

Quantitative textural parameters such as length, width, area, orientation and center position of crystals are systematically measured from 2D images (Sahagian and Proussevitch, 1998; Higgins, 2000). Based on these parameters, a mean 3D aspect ratio of crystals is calculated (Higgins, 2000; Morgan and Jerram, 2006) to apply it in all crystals of the sample regardless of its length. Considering a regular orientation of crystals, the resulting crystal lengths are distributed partitioning the crystal size axis in logarithmical or linear intervals defined by an arbitrary selected number of bins per decade (Higgins, 2000). Nevertheless, the 3D aspect ratio of crystals is a function of the undercooling (Lofgren, 1974; Shea and Hammer, 2013) and of the cooling rate (Pupier et al., 2008; Shea and Hammer, 2013). Consequently, the use of a same 3D crystal aspect ratio for all crystals in a system supposes a constant undercooling. Later, $n(L)$ is calculated as the differential of the cumulative crystal length (measured) distribution curve (N), thus no bin selection is needed.

The calculated 3D crystal size database could be applied using three kind of crystallization models: the open system model (Marsh, 1988) that considers an open system of constant volume with influx and outflux of magma and G independent of the initial crystal size (e.g, Kirkpatrick et al., 1979; Muncill and Lasaga, 1987; Marsh, 1998), the batch system model (Marsh, 1998) that considers a closed system and G independent of the initial crystal size, and the inversion of the CSD model (Melnik et al., 2011; Spillar and Dolejs, 2013) that uses $\varphi(t)$ as the input to calculate G and J. The first model

assumes constant *G* and *J* giving straight line CSDs, where *G* and *J* are calculated from the intercept and the slope of the CSD; the second model assumes a constant *G* and an exponentially increasing *J* giving convex CSDs with a *n*(*L*) peak different to the intercept, where *G* and *J* are calculated from an interpolation of the CSD intercept and the CSD slope of the longest crystals; and the last model calculates a exponentially decreasing *G* and a exponentially increasing *J* considering soft changes of the CSD slope, where *G* and *J* are calculated from *n*(*L*), the CSD slope and the maximum crystal size. The resulting *G* and *J* from any of these three models do not follow an asymmetrically bell-shaped curve with regard to the time or the undercooling like thermodynamic models show (e.g., Spohn et al., 1988; Hort and Spohn, 1991; Hort, 1997; Couch et al., 2003; Shea and Hammer, 2013).

For these reasons, we present a new procedure to develop CSD analysis based on the modeling of the cumulative distribution of crystal lengths considering it like a continuous and differentiable function. The resulted CSD is a convex curve that gives bell-shaped *G* and *J* curves and a sigmoidal *φ* with regard to the time comparable with the obtained from thermodynamic models. To verify the applicability of our model as in volcanic as in intrusive systems, the presented model is tested using plagioclase CSDs from the 1971 Villarrica Volcano lava flow and from the Qz-monzodiorites of the La Gloria Pluton.

Calculation of kinetic parameters from the new CSD procedure

The length-width ratio of crystals (*l*:*w*)(*l*) is a linear function of the crystal length (*l*) (Pupier et al., 2008) and is comparable to the small axis-intermediate axis ratio (Higgins, 2000; Pupier et al., 2008). We assume that crystals with the same area have the same length. We calculate the equivalent size (L_e) of any crystal *k* of *l* equals to l_k using the following expression:

$$L_e^k = \sqrt{A^k \times (l{:}w)(k)} \qquad (3.1)$$

Where A^k is the area of the crystal k. The cumulative distribution of crystal lengths is obtained using L_e and it is continuously modeled through the following error function

$$N(L_e) = a \times \mathrm{erf}(b \times L_e) + c \qquad (3.2)$$

Where a, b and c are constants. A partial population density ($n_p(L_e)$) can be calculated considering the relationship between N and n (Marsh, 1988)

$$n_p(L_e) = \frac{\partial N(L_e)}{\partial L_e} \qquad (3.3)$$

The CSD slope (S) is calculated as the differential of the CSD diagram

$$S(L) = \frac{\partial ln(n(L_e))}{\partial L_e} \qquad (3.4)$$

Based on empirical studies (Couch et al., 2003; Zieg and Lofgren, 2006) indicating that the crystal population density moves rightward in the CSD diagram by an increment ΔL in a Δt (Melnik et al., 2011; Spillar and Dolejs, 2013), the length increment (ΔL) is related to a time-dependent G determination as follow

$$\Delta L = \int_{t}^{t+\Delta t} G(\tau)\partial\tau \qquad (3.5)$$

The nucleated crystals in the same time interval are

$$\Delta N = \int\limits_{t}^{t+\Delta t} J(\tau)\partial\tau \qquad (3.6)$$

Our procedure requires finite discretization of the crystal length and of the crystallization duration domains to apply the numerical basis. The CSD crystal length scale is discretized into a regularly spaced sequence $\{L_i\}$, where $i \in \{0 \ldots N\}$ such that $L_0 = 0$, $L_{i+1} = L_i + \Delta t$ and L_N = Maximum crystal length. The crystal population density corresponding to the size i is $n_i = n(L_i)$. The crystallization duration is also discretized as $\{t_i\}$ with $i \in \{0 \ldots N\}$ where t_i corresponds to the duration when crystals of actual size L_i nucleated. Because the rightward advance of the CSD, $t_N = 0$ and $t_0 = t_{total}$, thus, the resulting kinetic parameters $J(t)$, $G(t)$ and $\varphi(t)$ according to the crystal length discrete values can be expressed as

$$J(t_i) = J_i \; ; G(t_i) = G_i \; ; \; \varphi(t_i) = \varphi_i \qquad (3.7)$$

Φ is calculated as a function of the crystal size modifying the expression of Marsh (1998) and Higgins (2002a) as

$$\varphi_i = \sigma \sum_{j=L_M-i}^{L_M} n_{j0} exp(-S_j(L_{mj} - L_M + i))(L_{mj} - L_M + i)^3 \Delta L \qquad (3.8)$$

Where σ is a crystal form parameter, L_M is the real maximum crystal length, L_{mj} is the mean size of the j interval and n_{jo} is the interpolation of the segment up to the intercept defined as

$$n_{j0} = n_j - \frac{n_j - n_{j+1}}{\Delta L} \times (L_j - N + j) \qquad (3.9)$$

The final calculated volume fraction is obtained with $i = 0$. The partial population density is moved until φ_0 were equal to the area fraction of all crystals (A) to obtain the final population density ($n(L)$). The variables φ^p, $\log(n^u(L))$, $\log(n^m(L))$ and $\log(n^l(L))$

are only created to apply in this algorithm. In the first step $\varphi^p = \varphi_o$. If $\varphi^p > A$, $\log(n^u(L))$ = $\log(n_p(L))$ and $\log(n^l(L)) = \log(n_p(L)) - 20$ (or a sufficient value 'α' such as $\varphi_o < A$ moving - α the $\log(n_p(L))$ function); or if $\varphi^p < A$, $\log(n^l(L)) = \log(n_p(L))$ and $\log(n^u(L)) = \log(n_p(L)) + 20$. For the following step, $\log(n^m(L))$ is the average between $\log(n^l(L))$ and $\log(n^u(L))$, φ^p is calculated for the $\log(n^m(L))$. If $\varphi^p > A$, $\log(n^u(L)) = \log(n^m(L))$ and the algorithm is repeated. If $\varphi^p < A$, $\log(n^l(L)) = \log(n^m(L))$ and the algorithm is repeated. If $\varphi^p = A$, $\log(n(L)) = \log(n^m(L))$ and the algorithm is ended (Figure 3.1). This algorithm changes the population density, without varying the CSD slope and the maximum crystal length.
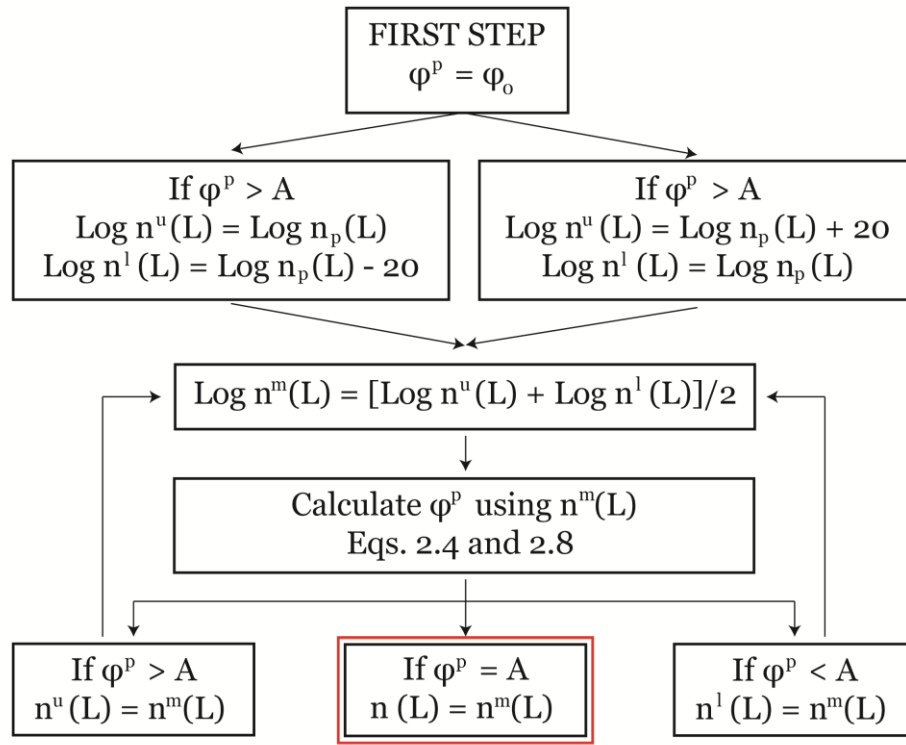
Figure 3. 1: Flow chart to calculate a population density such as the calculated crystal volumen fraction were equal to measured crystal área fraction.

G is calculated considering it proportional to S (Zieg and Lofgren, 2006; Pupier et al., 2008) as follow:

$$G_i = \frac{G_c \times S_i}{S_c} \qquad (3.10)$$

28

Where G_c is a characteristic crystal growth rate related to a characteristic CSD slope (S_c) and S_i is the CSD slope at the position i. G_c for a certain crystal size interval can be obtained through several methods such as heat balance models (e.g, Cashman, 1993; Marsh, 1996; Hort, 1997; Hawkesworth et al., 2000), cooling of lava flows or lava lakes (e.g., Cashman and Marsh, 1988; Cashman, 1993; Crisp et al., 1994; Cashman et al., 1999), Uranium-series isotopes (e.g., Condomines et al., 1988; Albarede, 1993; Sigmarsson et al., 2002; Hawkesworth et al., 2004), diffusion modeling (e.g, Zellmer et al., 1999; Davidson et al., 2001; Costa et al., 2003; Costa and Chakraborty, 2004; Morgan et al., 2004; Morgan and Blake, 2006) or using measured parameters from other CSD studies (e.g., Salisbury et al., 2008; Vinet and Higgins, 2010).

As the crystal population density of a certain crystal length corresponds to its nucleation density, the crystal nucleation rate is defined as

$$J_i = n_i \times G_i \tag{3.11}$$

The representative duration of crystallization is

$$t_i = \frac{\Delta L}{G_i} \tag{3.12}$$

And the total duration of crystallization is the sum of the duration of all intervals

$$t_{tot} = \sum_{i=1}^{L_M} t_i \tag{3.13}$$

Error Analysis

Inaccuracy in the determination of CSD analysis comes mainly from two sources. The first one is related to the image resolution. We have estimated that 2D crystal length can vary around 10 pixels using hand-marking technique. Consequently, the error will be higher for smallest crystals because the higher ratio between the length of 10 pixels and

the crystal length and their higher population density. This error (σ_1) can be quantified using the following formula

$$\sigma_1^k = \frac{n_{k-}^{k+}}{N_m} \qquad (3.14)$$

Where σ_1^k is the associated error to hand-marking technique in the crystal size k, N_m is the total number of measured crystals and n_k^{k+} is the number of crystals in the vicinity of 10 pixels for the crystal size k. σ_1 would not be higher to 5% for smallest crystals and negligible for longest crystals.

The second source of error is related to the regression of the error function applied to the calculation of N. This error would not be higher than 2%. Consequently, the analytical error of our procedure should not be higher than 7% for smallest crystals and 2% for longest crystals.

Discussion

Stereology

The stereological crystal conversion is difficult if it is necessary assume a 3D crystal aspect ratio because the morphology, elongation and arrangement of crystal are functions of the undercooling and the cooling rate (Lofgren, 1974; Pupier et al., 2008; Shea and Hammer, 2013) having longer crystals with higher undercooling and higher cooling rates. Empirically, 3D k-feldspar and quartz textural data of porphyritic rhyolite from the Late Paleozoic Halle Volcanic Complex has been obtained using X-ray tomography (Mock and Jerram, 2005; Jerram and Higgins, 2007). The measured 3D mean aspect ratio in k-feldspar was 1:1.6:2.8 with a small/intermediate axis ratio error of 26.7% and a small/large axis ratio error of 41.1%. The measured 3D mean aspect ratio in quartz was 1:1.3:1.7 with a small/intermediate axis ratio error of 15.6% and a small/large axis ratio error of 20.7% (Figure 3.2). Both minerals, regardless of their mean elongation, showed a large scattering and standard deviation in their aspect ratios. Consequently, the use of the same 3D crystal aspect ratio for a whole sample is a wrong

assumption and the calculation of the probability of cutting in crystal corners is impossible.

A good consideration is that the intermediate axis – small axis ratio is a linear function of crystal length (Pupier et al., 2008). This ratio and the measured crystal area can be used to calculate the crystal size with lower uncertainty. The use of 2D textural parameters to decipher magmatic processes has been increasing in the last years (e.g., Couch et al., 2003; Toramaru, 2006; Toramaru et al., 2008; Noguchi et al., 2008; Salisbury et al., 2008; Preece et al., 2013) guaranteeing the reliability of our procedure.
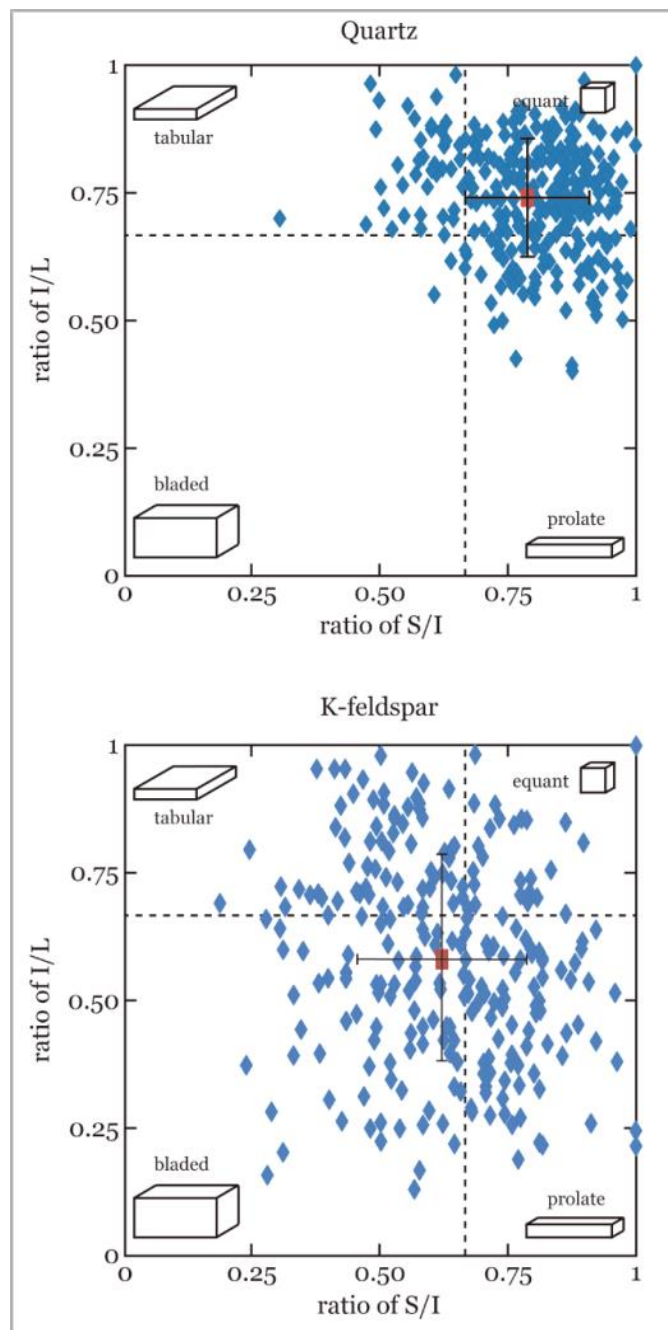
Figure 3. 2: 3D measured aspect ratios of Quartz and K-feldspar from the Late Paleozoic Halle Volcanic Complex (Mock and Jerram, 2005; Jerram and Higgins, 2007) plotted in a Zingg diagram (Zingg, 1935). Quartz shows a S/I ratio of 0.7883 ± 0.1233 and a I/L ratio of 0.7400 ± 0.1141 that corresponds to a S:I:L of 1:1.27±0.20:1.72±0.36. K-feldspar shows a S/I ratio of 0.6198 ± 0.1655 and a I/L ratio of 0.5811 ± 0.2030 that corresponds to S:I:L of 1:1.61±0.43:2.82±1.16. These high standard deviations of 3D measured aspect ratios show there is not a common 3D aspect ratio in nature. Consequently, the use of unique 3D mean aspect ratio is not adequate to do CSDs.

The partition of N

The next step to develop CSD analysis is the calculation of the crystal population density as a function of the crystal size. The crystal population density can be directly obtained measuring the amount of crystals in a unit of volume (e.g., Higgins, 2000) or calculating the slope of the cumulative distribution of crystal lengths curve (e.g., Cashman and Marsh, 1988). Conventionally, regardless of the method used, the crystal size axis has been partitioned in an arbitrary number of bins per decade using logarithmical or linear distribution. CSD diagrams could indicate substantially different values of crystallization parameters if the selected number of bins is changed. To illustrate the effect of the selected number of bins per decade on CSD analysis, we use a basaltic andesite lava sample of the 1971 Villarrica volcano eruption (Moreno and Clavero, 2006). Plagioclase phenocrysts were hand- marked from a scanned thin section image of 3.5 x 2.5 cm and plagioclase microcrysts were hand-marked from a BSEM image with a focus of 200X. The scanned thin section image has 1569 plagioclase crystals with a length from 64 μm to 2705 μm. The BSEM image has 1444 plagioclase crystals with a length from 3 μm to 120 μm. The software CSDCorrections 1.40 was used to convert 2D data in 3D data (Higgins, 2000). A mean 3D crystal aspect ratio of 1.0:2.7:4.0 was calculated by the software CSDSlice (Morgan and Jerram, 2006) that corresponds to the calculated aspect ratio of phenocrysts. A roundness index of 0.1 and a fabric index of 0.3 were input. Four, seven and ten bins per decade in a logarithmical distribution on base 10 were selected for comparison. The output of CSDCorrections software is interpolated using third-degree polynomial regressions. The resulting G, J, t and φ of CSD diagrams were calculated using the Spillar and Dolejs's treatment (2013).

The maximum crystal length obtained from CSD diagrams using the three numbers of bins per decade has a standard deviation of 14%. In addition, the position of the kink in CSD diagrams has a standard deviation of 24%. The nucleation density does not substantially vary showing a variation of 3% (Figure 3.3). Only the CSD diagram of ten bins per decade shows a decreasing crystal population density with decreasing crystal size in the three smallest bins. t of the complete magmatic process shows a variation of 34% considering the three cases. t for the segment previous to the kink varies a 60% (Figure 3.4) and the initial crystal growth rate varies a 79% (Figure 3.5). Every case present differences in crystal growth rate trend before and after the kink

(Figure 3.5). The crystal nucleation rate and the crystal volume fraction are not significantly affected by the number of bins per decade.
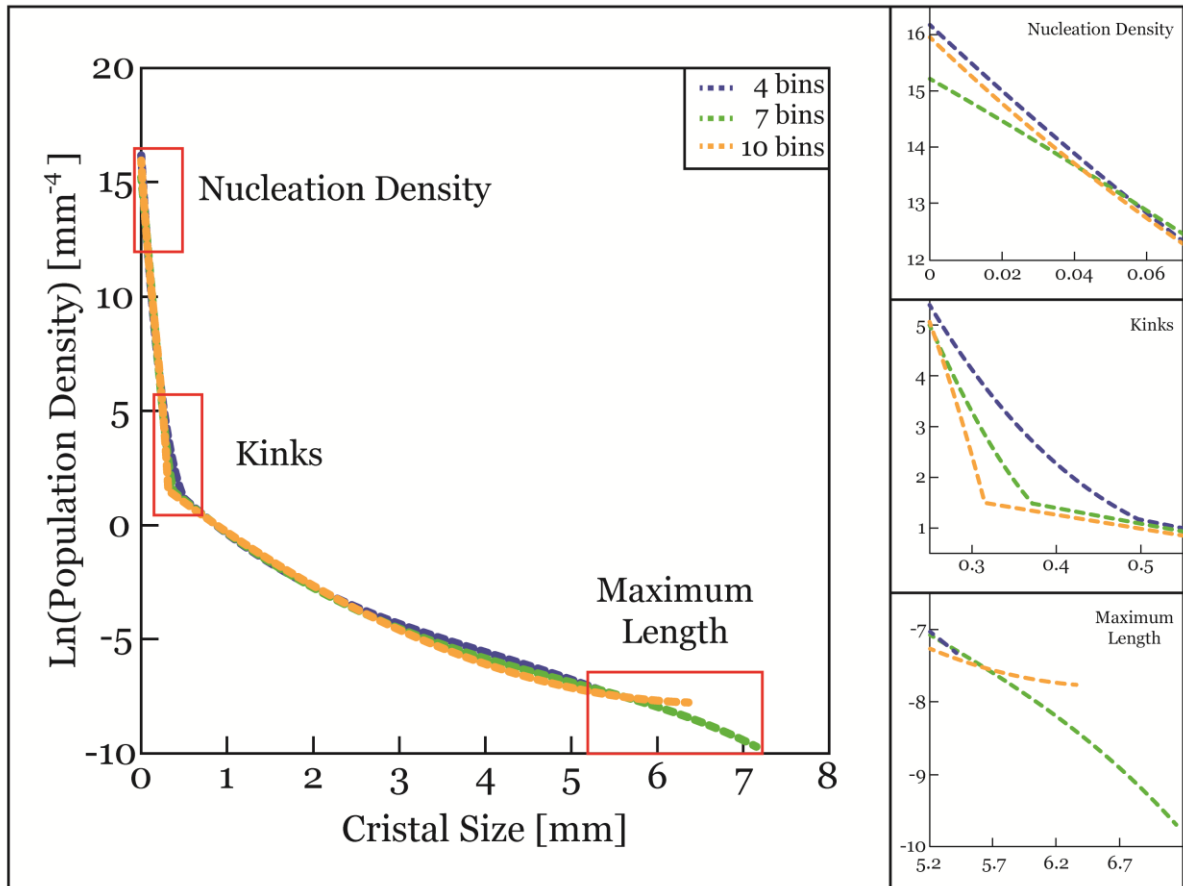
Figure 3. 3: CSDs of the 1971 Villarrica Volcano lava flow sample using 4, 7 and 10 bins per decade. The maximum crystal length (L_M), the position of the kink and the nucleation density (n_o) vary if the number of bins per decade is changed. The CSD of 4 bins per decade presents a L_M of 5.41 mm, a Ln(L_M) of -7.33, a kink located at 0.497 mm with a Ln(n) of 1.17 and a Ln(n_o) of $e^{16.17}$; the CSD of 7 bins per decade presents a L_M of 7.15 mm, a Ln(L_M) of -9.70, a kink located at 0.372 mm with a Ln(n) = 1.49 and a Ln(n_o) of $e^{15.21}$; the CSD of 10 bins per decade presents a L_M of 6.36 mm, a Ln(L_M) of -7.76, a kink located at 0.315 mm with a Ln(n) = 1.52 and a Ln(n_o) of $e^{15.95}$.
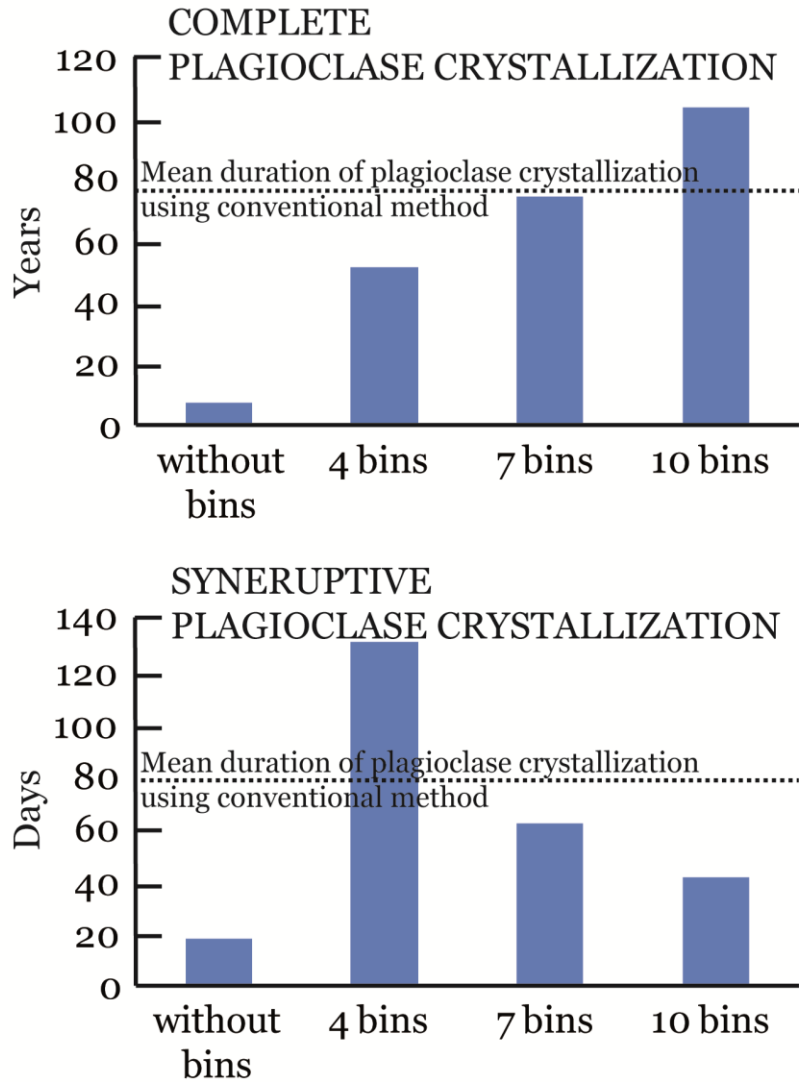
Figure 3. 4: Crystallization duration histograms for the complete crystallization process and for the syn-eruptive stage of the 1971 Villarrica Volcano lava flow using 4, 7 and 10 bins per decade. The duration of crystallization is strongly affected if the number of bins per decade is changed. *t* is 51.12 y, 74.54 y and 103.62 y for the complete crystallization process with 4, 7 and 10 bins per decade respectively and 130.61 d, 61.61 d and 41.34 d for the syn-eruptive stage with 4, 7 and 10 bins per decade respectively. The dashed line is the average of the three cases for both histograms.
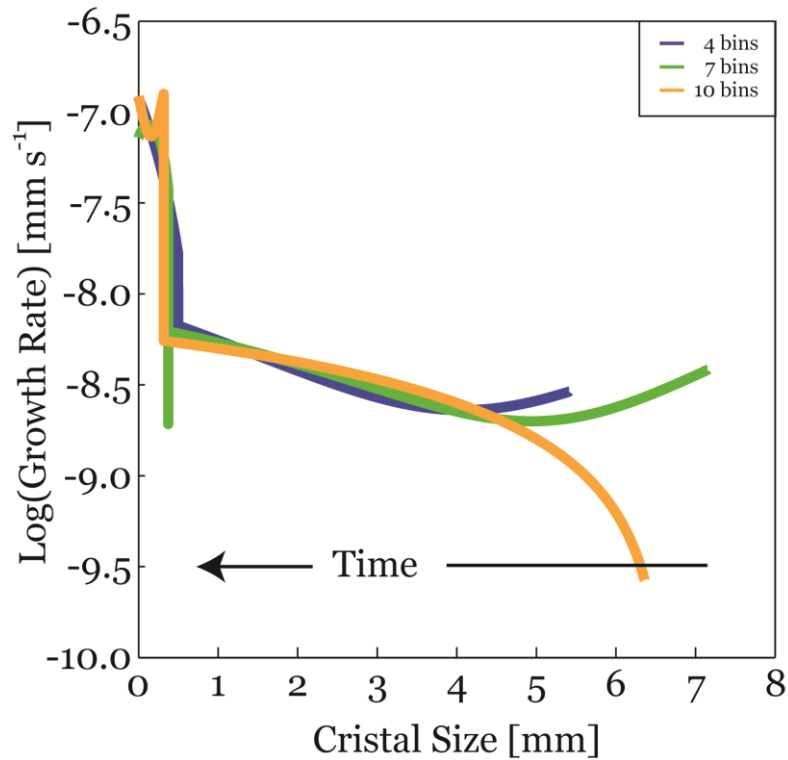
Figure 3. 5: Calculated *G* based on CSD of the 1971 Villarrica Volcano lava flow using 4, 7 and 10 bins per decade. *G* is calculated as a function of *t* and *L* using the Spillar and Dolejs's procedure (Spillar and Dolejs, 2013) and relating a *G* of 2 x 10^{-8} mm s^{-1} with a *S* of 10.12. The x-axis is crystal length because the syn-eruptive stage is not visible using the crystallization duration. The initial *G* (*G$_i$*) varies if the number of bins per decade changes. The case of 4 bins per decade has a *G$_i$* of 2.90 x 10^{-9} mm s^{-1}, the case of 7 bins per decade has a *G$_i$* of 3.81 x 10^{-9} mm s^{-1} and the case of 10 bins per decade has a *G$_i$* of 2.67 x 10^{-10} mm s^{-1}. *G* shows concave curves with 4 and 7 bins per decade and continuously increasing convex curve with 10 bins per decade during the pre-eruptive stage and it shows a continuous increasing curve with 4 bins per decade, a convex curve with 7 bins per decade and a concave curve with 10 bins per decade during syn-eruptive stage.

Applications

The 1971 Villarrica Volcano eruption

The Villarrica Volcano is a stratovolcano located in the south of Chile, in the Central Southern Volcanic Zone of the Andes (39° 24' S). Its activity has lasted from Middle Pleistocene to the present forming from basalts to andesites. Since 1787, their eruptions have shown from strombolian to hawaiian paroxysms, forming a'a and pahoehoe lavas. The eruption of 1971 was an eruptive cycle that lasted from October to February. Its paroxysm was strombolian type, forming two lava flows towards the SW and NE flanks. The SW lava flow reaches 16.5 km-long with a variable height between 1

to 5 m. Samples from this lava flow are basalts to basaltic andesites with phenocrysts of Plagioclase, Olivine, Clinopyroxene and Orthopyroxene. The groundmass is formed by plagioclase, clinopyroxene, olivine and Fe-Ti oxides (Moreno and Clavero, 2006). The CSD was made based on plagioclase phenocrysts and microcrysts.

The CSD based on cumulative distribution curve of plagioclase was calculated from the two different scale images. L_M of 2.706 mm, $n(L_M)$ of $e^{-25.65}$ and n_o of $e^{12.10}$ were calculated using our procedure. The crystal population density corresponding to the kink at 0.099 mm is $e^{1.70}$ (Figure 3.6) and the calculated t for the syn-eruptive stage is *c.a.* 18 days and for the complete process is *c.a.* 7 years (Figure 3.4). φ varies sinuously with respect to t in the pre-eruptive stage reaching up to 0.2, whereas φ in the syn-eruptive stage increases abruptly up to 0.45 (Figure 3.7). G, calculated from eq. 3.10 with G_c value of 2×10^{-8} mm s^{-1} and S_c of 10.12, decreases progressively more than one order of magnitude during the pre-eruptive stage. On the other hand, G increases up to two orders of magnitude at the beginning of the syn-eruptive stage (Figure 3.8). J varies with time following an asymmetrical gaussian distribution in both pre- and syn-eruptive stages and the ratio between the lowest and highest J values is about 10^{11} and 10^{6} for the pre- and syn-eruptive stage, respectively (Figure 3.8).
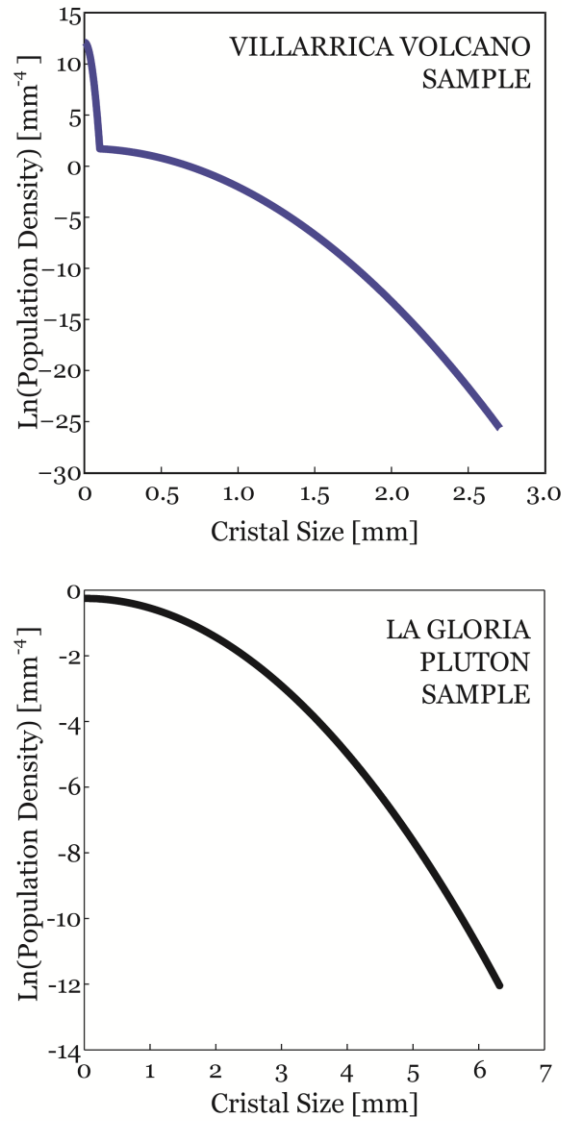
Figure 3. 6: Calculated CSD of the 1971 Villarrica Volcano lava flow sample and of the La Gloria Pluton sample based on the modeled cumulative distribution curves. Both axes are not equals because the big difference between parameters of both samples. In the Villarrica Volcano sample, L_M of 2.706 mm, $n(L_M)$ of $e^{-25.65}$ and n_o of $e^{12.10}$ were calculated. The crystal population density corresponding to the kink at 0.099 mm is $e^{1.70}$. In the La Gloria Pluton sample, L_M of 6.320 mm, $n(L_M)$ of $e^{-12.05}$ and n_o of $e^{-0.25}$ were calculated.
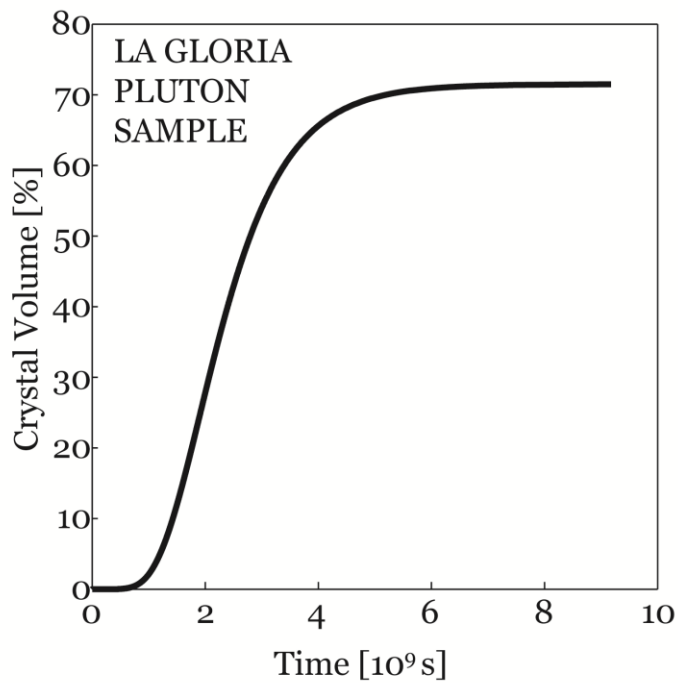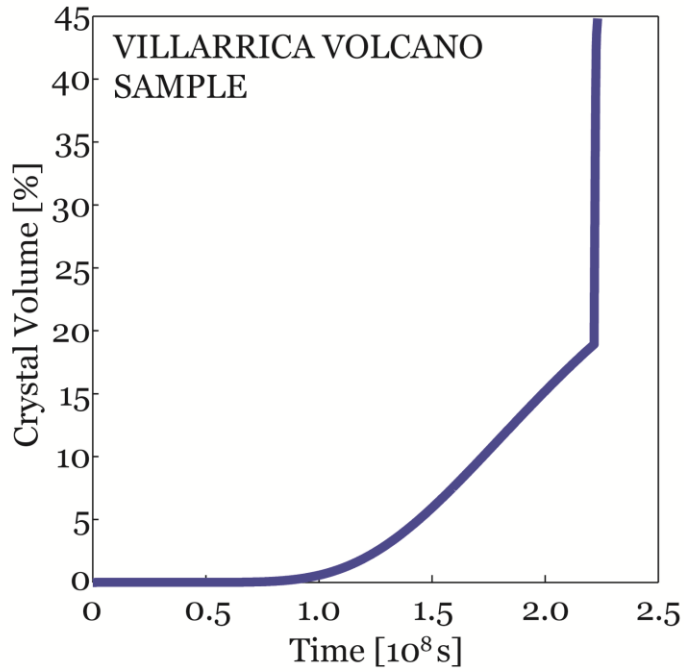
Figure 3. 7: φ as a function of time for the Villarrica Volcano sample and for the La Gloria Pluton sample. Both axes are different because the big differences in the values of both samples. The pre-eruptive stage of the Villarrica Volcano sample has a sinuous form followed by a steep increase. The La Gloria Pluton sample has a perfect sigmoidal form showing that, previous to the total crystallization, φ is very stable during a long time interval because of the little available volume to crystallize.
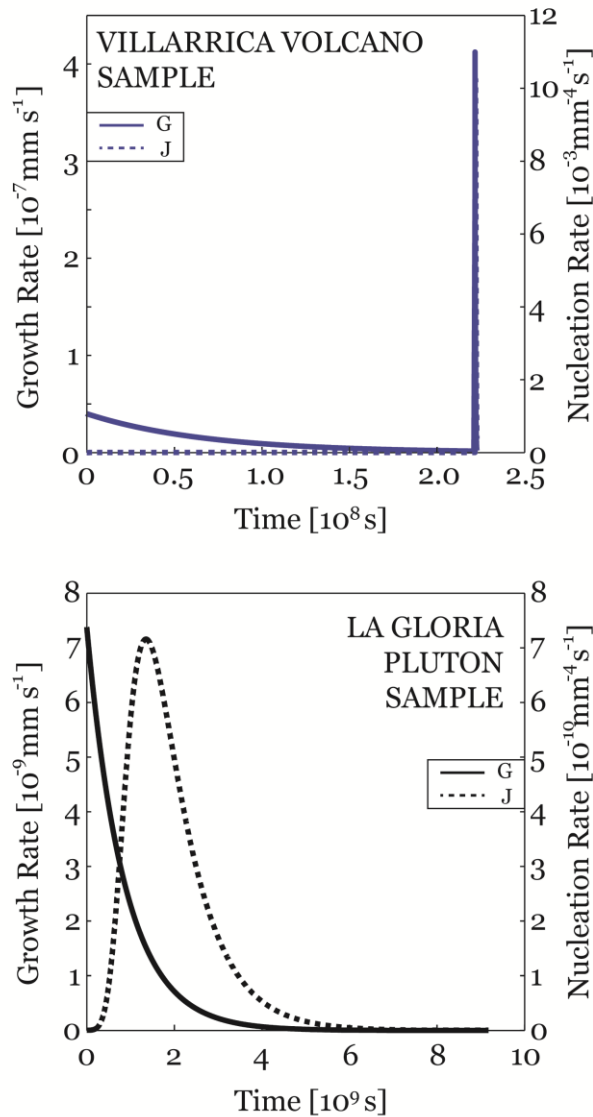
Figure 3. 8: *G* and *J* as functions of the time for the Villarrica Volcano sample and the La Gloria Pluton sample. Both y-axis and the x-axis are not equals because the big difference between samples. Both crystallization rates increase sharply during the last stage of crystallization in the Villarrica Volcano sample. Both crystallization rates of the La Gloria Pluton sample show similar paths to shown in thermodynamic studies having asymmetrical gaussian distributions. The peak of *G* is followed by the peak of *J* such as in numerical models.

The maximum plagioclase length using our method is approximately 2 times smaller than calculated by CSDCorrections and the plagioclase crystal length at the kink is 3 to 5 times smaller. Both textural data are consistent with the maximum length of plagioclase pheno and microcrysts recorded in the studied sample (Figure 3.9). According to the equation 3.13, the calculated duration of crystallization is a function of the crystal length. In this case, the calculated 7 years for the complete plagioclase crystallization is 8 to 14 times lower than calculated using the conventional method and

coincides with the time interval that separate the 1971 eruption with the previous one (1964) (Moreno and Clavero, 2006). *G* and *J* with regard to the time have asymmetrical bell-shaped distributions before and after the kink. Our method shows how an eruption violently affects the crystal kinetic parameters with sharp increases of *G*, *J* and *φ* in $10^{2.2}$, 10^7 and 2.25 times from pre-eruptive to syn-eruptive stage respectively. G with regard to the time calculated using the conventional method depends on the number of bins per decade showing different trends that would imply different processes affecting to the magma such as a decrease in the available volume (Spillar and Dolejs, 2013), an increase in the undercooling rate due to water exsolution (Cashman and Blundy, 2013), a change in temperature due to variations of latent heat (Blundy et al., 2006) or water exsolution during ascent magma (Shea and Hammer, 2013). Regardless of the number of bins per decade, CSDs calculated by the conventional method do not express the sharp increase on *G* and *J* due to eruptions and the peak of both crystallization rates is lower than expected results (Cashman, 1993; Hammer et al., 1999; Cashman and Blundy, 2000; Blundy and Cashman, 2005).
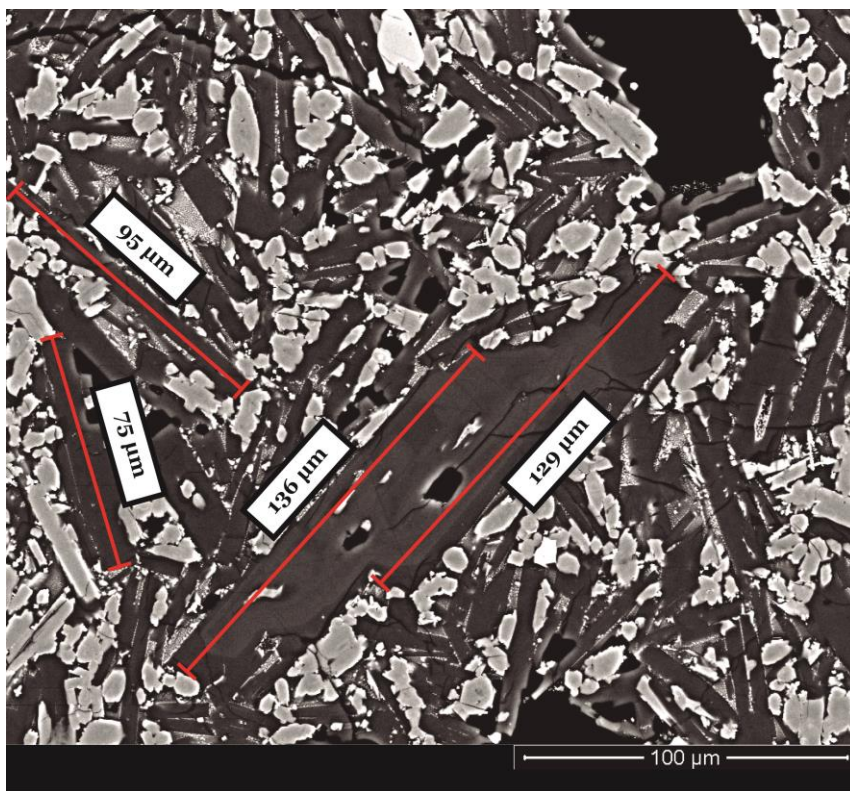
Figure 3. 9: BSEM image of the 1971 Villarrica Volcano sample. Four plagioclases were measured in the image showing that longest microcrysts, identified for their high elongation, are smaller than 100 µm. On the other hand, smallest phenocrysts, identified for their complex zoning pattern, are longer than 120 µm.

La Gloria Pluton

The Pluton La Gloria is an epizonal intrusion located 40 km eastward from Santiago, Chile (33° S). It belongs to a N-S belt compound by granodioritic to qz-monzonitic intrusions with a data from middle to upper Miocene. This intrusion presents an elongated form of NNW orientation, with 20 km –long, a width between 3 and 6 km and an exposed height of 2.5 km. Pluton La Gloria presents five zones according to its composition and textures: 1) The lower-central zone is compound by granodiorite and qz-monzodiorite, 2) The lower-rim zone is compound by granodiorite and qz-monzodiorite with a higher volume of hornblende, 3) The center zone is compound by qz-monzodiorite and qz-monzonite, 4) The central-rim zone is compound by qz-monzodiorite and qz-monzonite with higher crystal sizes and 5) The upper zone is comppund by qz-monzonite. All rocks are formed by plagioclase, quartz, pyroxene, hornblende, biotite, k-feldspar, Fe-Ti oxides, apatite and titanite (Cornejo and Mahood, 1997). The CSD was made based on plagioclase from several samples of qz-monzodiorite.

The plagioclase CSD was made supposing an only one and continuous crystallization. Plagioclases were hand-marked from a scanned thin section image where 696 crystals were found with a length from 0.290 mm to 6.320 mm. The resulting CSD is a continuous and convex curve with n_o of $e^{-0.25}$ and $n(L_M)$ of $e^{-12.05}$ (Figure 3.6). The total duration of crystallization used was 4000 years, the intermediate duration presented by Gutierrez et al., (2013). Both crystal kinetic rates present asymmetrical gaussian distributions: G varies from 5.37×10^{-10} mm s^{-1} to 4.25×10^{-14} mm s^{-1} and J begins with a rate of 3.14×10^{-15} mm^{-4} s^{-1}, reaching a peak of 5.21×10^{-11} mm^{-4} s^{-1} and decreasing up to 3.29×10^{-14} mm^{-4} s^{-1} (Figure 3.8). φ has a sigmoidal form, it is stable during the first 330 years, later it increases sharply up to 2220 years reaching almost the final φ and it is almost stable in the last 1450 years with a φ of 0.70 (Figure 3.7).

The resulting convex CSD is very similar to CSD curves obtained by Batch system model (Marsh, 1998) that calculates crystal population densities considering a constant G and an exponentially increasing J. On the other hand, our procedure calculates asymmetrical gaussian distributions of G and J with regard to the time, where the peak of the former is always previous to the peak of the latter such as it has described in numerical and experimental models (Spohn et al, 1988; Hort and Spohn, 1991; Hort,

1997; Couch et al., 2003). The sigmoidal form of the calculated time-dependent φ is very similar to the obtained φ by theoretical and experimental models (Avrami, 1939; Avrami, 1940; Kirkpatrick, 1976). The first stable stage coincides with the *G* peak considering an initial φ equals to zero. The second stage characterized by a sharp increase of φ coincides with the *J* peak that is consistent with the strong crystal nucleation dependence of φ related to magmatic processes of high nucleation of crystals such as magma ascent, water exsolution or high undercooling rates (e.g., Couch et al., 2003; Blundy et al., 2006; Pupier et al., 2008; Cashman and Blundy, 2013; Shea and Hammer, 2013). Finally, the third stage shows a final stable crystal volume fraction of 0.7 where magmatic systems can be considered like mush-type reservoirs (e.g, Bachmann and Bergantz, 2004). In reservoirs with $\varphi > 0.5$, crystals are almost in contact, decreasing the possibility to form new nuclei or to regrowth previous crystals regardless of the temperature and water pressure conditions (Marsh, 1998; Resmini, 2007; Spillar and Dolejs, 2013) (Figure 3.10).
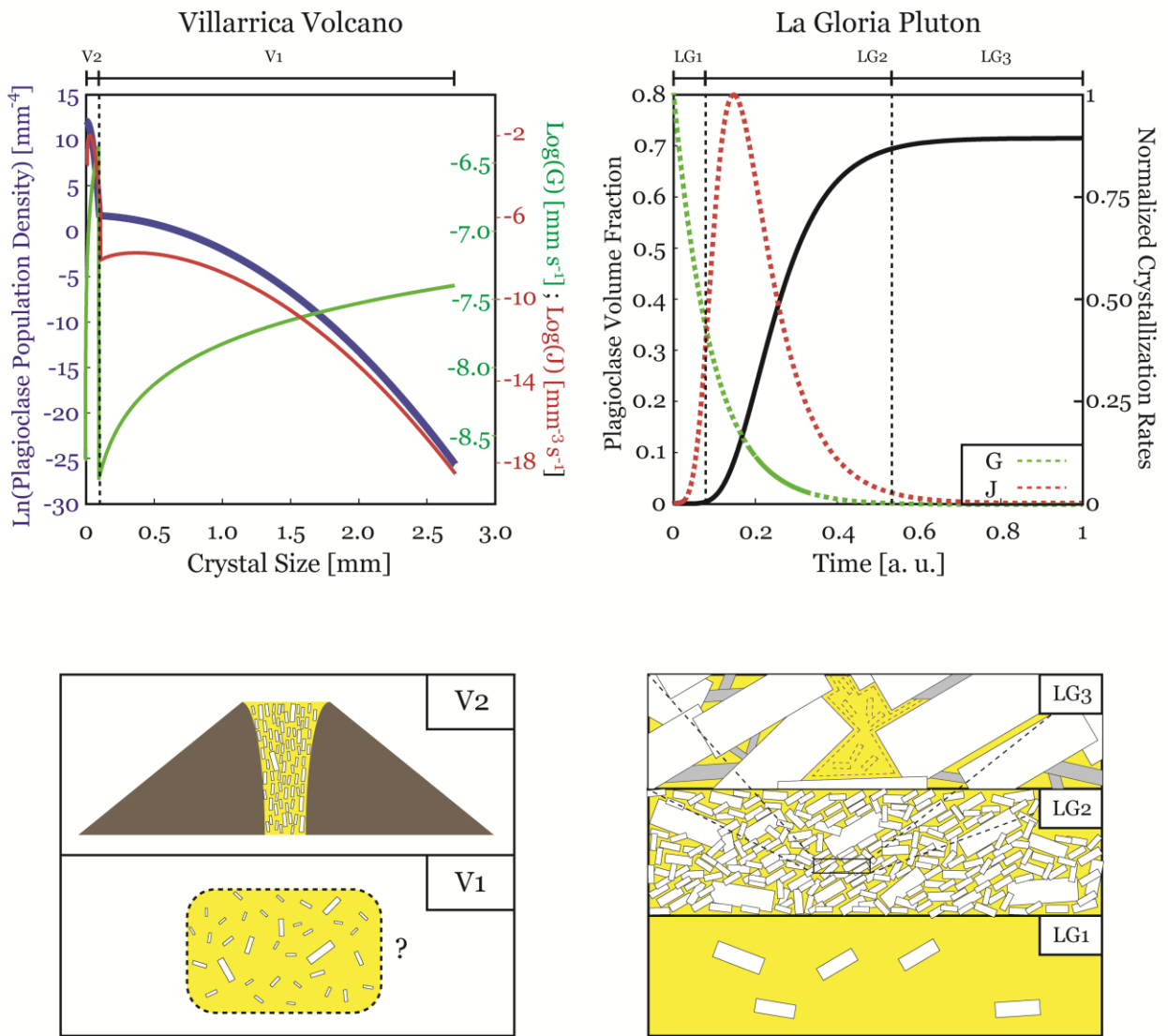
Figure 3. 10: Comparison between crystallization rates and the CSD of the 1971 Villarrica Volcano sample and comparison between normalized crystallization rates and plagioclase volume fraction of the La Gloria Pluton sample. G continuously decreases against an almost continuous increase of J during the pre-eruptive stage for the 1971 Villarrica Volcano sample. Both crystallization rates and the population density sharply increase because of magma ascent. On the other hand, the crystallization process of the La Gloria Pluton can be divided in three stages according to the φ path: a first stage of low crystallization forms a few of crystals because a high G and a low J, later a second stage shows a strong increase of φ corresponding to the peak of J, and finally, both crystallization rates decrease because of the small available space to form new nuclei or regrowth previous crystals.

Conclusion

The current work presents a new method to calculate crystal size distributions with the objective of obtaining crystal growth and nucleation rate paths more similar to

expressed by numerical and experimental thermodynamic works. The measured quantitative textural parameter database is not converted to 3D crystal sizes using probabilistic models (Saltikov, 1967; Higgins, 2000) because these need an input of a unique crystal aspect ratio. The morphology of crystals varies with the variation of the undercooling and with the variation of the cooling rate (Lofgren, 1974; Shea and Hammer, 2013) giving a final high scattering of empirical crystal aspect ratios (Mock and Jerram, 2005; Jerram and Higgins, 2007).

In this work, the cumulative distribution of crystal length function is not discretized in intervals logarithmically distributed because this method biases the calculation of the population density. CSDs were calculated using 4, 7 and 10 bins per decade using a logarithmical distribution obtaining a standard deviation with regard to the average of 13.8% for the maximum crystal length, 23.6% for the position of the kink and 3.2% for the nucleation density. These scatterings affect the resulting duration of crystallization of pre-eruptive stage, the resulting duration of crystallization of syn-eruptive stage and the initial crystal growth rate obtaining a standard deviation with regard to the average of 34.4%, 60.1% and 79.1% respectively.

Consequently, CSDs are modeled based on measured crystal lengths focusing on the cumulative distribution of crystal length function, the integral of the population density that is continuously modeled using an error function. Considering that G is proportional to the CSD slope and that the time advances leftward in the CSD diagram, G, J and φ are obtained as a function of the time. The calculated duration of crystallization was very similar to the time interval between the presented and its previous eruption and as G as J show an instantaneous increase just after of the eruption. A plutonic system was also modeled showing asymmetrical gaussian distributions of G and J with regard to the time, with the G peak previous to the J peak. The calculated φ shows a sigmoidal curve with regard to the time. This form can be interpreted as three stages of crystallization: a first stage of a very low increase of crystallization corresponding to the G peak, a second stage of a sharp increase of crystallization corresponding to the J peak and a final stage of soft increase of crystallization due to the small available space to create new nuclei or to regrowth previous crystals.

Finally, the use of measured textural parameters to do CSD analysis increases the possibility of coupling this technique with other ones to decipher magmatic processes. The quantitative textural analysis with regard to the crystal size could be followed by the qualitative textural analysis of the same crystals such as zoning (e.g., Murphy et al., 2000; Bouvet de Maisonneuve et al., 2013), disequilibrium textures (Tsuchiyama, 1985; Cashman and Blundy, 2013) or the form of crystal rims (Tsune and Toramaru, 2007) that reveal how crystal grew (or dissolved). The mineral composition (X) can be measured through 2D profiles (e.g., Salisbury et al., 2008; Vinet and Higgins, 2010; Bouvet de Maissoneuve et al., 2012) that allows express X as a function of crystal size, such as CSD allows with G and J. Consequently, X could be mathematically related with G or J through L using CSD analysis to decipher thermodynamic conditions in which crystals formed (e.g, Lasaga, 1982; L'Heureux, 1993).

Capítulo 4

Solving magmatic T – P$_{H2O}$ conditions through plagioclase CSDs and anorthite content

Manuscrito para ser sometido en la revista Contributions to Mineralogy and Petrology

Abstract

Crystal size distribution analysis can be coupled with other numerical parameters to constrain magmatic processes with a higher resolution. The anorthite content in plagioclase can be expressed as function of the crystal size in the same way of the calculated crystal growth rate, the crystal nucleation rate and the volume fraction of crystals by CSD. As the plagioclase composition as crystal kinetic parameters are functions of thermodynamic parameters such as the temperature and the water pressure. Using a crystal volume fraction - undercooling relationship, the calculation of the liquidus temperature as a function of the water pressure and an anorthite content - temperature - water pressure relationship, the temperature and the water pressure can be calculated. The model is applied in volcanic products of the 1915 Lassen Peak Volcano eruption. Two heating events previous to the eruption are inferred. The latter is because of the mixing of the dacitic magma with an andesitic magma. A stable stage follows the first heating event showing a P$_{H2O}$ of 199 Mpa, a T of 830 °C forming plagioclase of anorthite content of 0.37. The magma mixing is followed by a second stable stage of a P$_{H2O}$ of 76 Mpa, a T of 959 °C and forming plagioclase of anorthite content of 0.68. A devolatilization process occurs just previous to the eruption. From the first stable stage, a minimum depth of 7 km is calculated. According to CSD calculations, the magma ascent lasts 18 hours. Thus, a magma ascent rate of 0.11 m s-1 was calculated. In summary, seven magmatic stages were recognized, distinguishing heating events, stable

stages and magma mixing into the pre-eruptive stage and magma ascent from the surface crystallization into the syn-eruptive stage.

Introduction

Igneous thermodynamic data have been usually obtained from geothermobarometers and hygrometers models (e.g., Putirka, 2008; Lange et al., 2009). Based on these singular data and the whole melt composition, thermodynamic paths are obtained using numerical thermodynamic softwares (e.g., Ghiorso and Sack, 1995; Holland and Powell, 2003). Calculated mineral compositions are compared with real mineralogy to check if the result model is consistent (e.g., Riker et al., 2009; Lohmar et al., 2012, Ustunisik et al., 2014). The crystal volume fraction and quantitative textural parameters are secondary results.

Quantitative textural parameters are usually measured in igneous rocks to apply their on Crystal Size Distribution (CSD) analysis (Marsh, 1988) that compares the population density of crystals with their size. The slope and the intercept of these diagrams have been used to calculate the crystal nucleation rate (J) and the crystal growth rate (G) (e.g., Cashman and Marsh, 1988; Marsh, 1998) and the existence of kinks or concave curves has been used to conclude different magmatic stages (e.g., Armienti et al., 1994) or mechanical processes affecting the crystallization (e.g., Spillar and Dolejs, 2015).

Both crystallization rates have been related with thermodynamic parameters. G and J show asymmetrical bell-shaped curves with regard to the undercooling (e.g., Spohn et al., 1988; Hort., 1997; Couch et al., 2003) and both rates have an exponential dependence with the cooling rate (Marsh, 1988; Cashman, 1993). The crystal volume fraction (φ) has been also related with the undercooling through almost linear functions (e.g., Marsh, 1981; Riker et al., 2009). There are some approaches to express plagioclase kinetic parameters as functions of temperature (T) and anorthite content (X_{An}) limited to anorthite-albite solid solutions (Kirkpatrick et al., 1979; Lasaga, 1982). On the other hand, the anorthite content has been expressed in several thermodynamic models as function of thermodynamic parameters (e.g, Bowen, 1913; Yoder and Tilley, 1962; Smith, 1972; Tsuchiyama and Takahashi, 1983; Schmidt et al., 2008; Cashman and Blundy,

2013). Despite of the clear $G - T$- X_{An} relationship, there is no studies that coupling CSD with obtained mineral composition to calculate thermodynamic paths, but some approaches that relate qualitatively quantitative textural parameters with mineral composition (Salisbury et al., 2008; Vinet and Higgins, 2010).

In the current work, the crystal volume fraction – undercooling relationship is used (Hort, 1997) inputting the calculated φ by CSD analysis. The liquidus temperature is calculated as a function of the water pressure (Cashman and Blundy, 2013). Moreover, the anorthite content – temperature – water pressure relationship is used (Cashman and Blundy, 2013) inputting measured plagioclase composition to calculate the crystallization temperature. Thus, a $X_{An} - T - P_{H2O} - \varphi - G - J$ path is obtained from the coupling of plagioclase CSD analysis and the anorthite content allowing the interpretation of magmatic processes with a higher accuracy than only using quantitative textural analysis.

To verify its applicability, the presented model is tested with plagioclase CSDs from different products and plagioclase composition database of the 1915 Lassen Peak volcano eruption from Salisbury et al.'s work (2008).

Numerical basis

Crystal kinetic parameters

Salisbury et al., (2008) develop plagioclase CSDs using the Wager formula to convert the areal population density ($n_A(l)$) in volumetric population density $n_V(L)$

$$n_V(L_{XY}) = n_A(l_{XY})^{1.5}$$

(4.1)

The goal of this formula is not to change the measured crystal size. To consider the variable time on CSD analysis, such that in Chapter 2, the crystal population density moves rightward in the CSD diagram by an increment ΔL in a Δt (Melnik et al., 2011; Spillar and Dolejs, 2013), where the length increment (ΔL) is related to a time-dependent G determination as follow

$$\Delta L = \int_{t}^{t+\Delta t} G(\tau)\partial\tau \qquad (4.2)$$

The nucleated crystals in the same time interval are

$$\Delta N = \int_{t}^{t+\Delta t} J(\tau)\partial\tau \qquad (4.3)$$

The same finite discretization of the crystal length and of the crystallization duration domains of the Chapter 2 is applied such that the resulting kinetic parameters $J(t)$, $G(t)$ and $\varphi(t)$ according to the crystal length discrete values are expressed as

$$J(t_i) = J_i \; ; G(t_i) = G_i \; ; \; \varphi(t_i) = \varphi_i \qquad (4.4)$$

And φ is calculated with the same equation

$$\varphi_i = \sigma \sum_{j=L_M-i}^{L_M} n_{j0} exp(-S_j(L_{mj} - L_M + i))(L_{mj} - L_M + i)^3 \Delta L \qquad (4.5)$$

G, J and t are calculated according to the following equations

$$G_i = \frac{G_c \times S_i}{S_c} \qquad (4.6)$$

$$J_i = n_i \times G_i \qquad (4.7)$$

$$t_i = \frac{\Delta L}{G_i} \qquad (4.8)$$

And the total duration of crystallization is the sum of the duration of all intervals

$$t_{tot} = \sum_{i=1}^{L_M} t_i \qquad (4.9)$$

Introducing thermodynamic and plagioclase composition parameters

As plagioclase crystals grow, anorthite content is recorded. Due to this obvious statement, the anorthite content can be considered as a numerical parameter using the same finite discretization of kinetic parameters, recording the anorthite content as $\{X_{Ani}\}$, where $i \in \{0 \dots N\}$ such that X_{Ano} = the rim composition, $X_{Ani+1} = X_{Ani} + \Delta t$ and X_{AnN} = the core composition. Other thermodynamic parameters such as the crystallization temperature (T), the liquidus temperature (T_l) and the water pressure (P_{H2O}) are parameterized using the same procedure. Thus, measured and calculated thermodynamic parameters $X_{An}(t)$, $T(t)$, $T_l(t)$ and $P_{H2O}(t)$ according to the crystal length discrete values can be expressed as

$$X_{An}(t_i) = X_{An_i} \; ; \; T(t_i) = T_i \; ; \; T_l(t_i) = T_{l_i} \; ; \; P_{H2O}(t_i) = P_{H2O_i} \qquad (4.10)$$

For following equations, the term undercooling (ΔT^u) is the difference between T_l and T and the solidus temperature (T_s) will be considered as a function of T_l (Cashman and Blundy, 2013)

$$T_s = T_l - 255 \qquad (4.11)$$

The relationship between T and φ (Hort, 1997)

$$\Delta T_i^u = 255 - \frac{255 \times \arccos(2\varphi_i - 1)}{\pi} \qquad (4.12)$$

T_l is a third-degree polynomial function of P_{H2O} if the whole melt composition does not vary

$$T_{l_i} = c_0 + c_1 P_{H2O_i} + c_2 P_{H2O_i}^2 + c_3 P_{H2O_i}^3 \qquad (4.13)$$

Where T_l is in ⁰C and P_{H2O} is in MPa. X_{An} is mainly a function of temperature and water pressure (Putirka, 2008; Rutherford and Devine, 2008; Lange et al., 2009; Ustunisik et al., 2014) and it can be expressed as

$$X_{An_i} = k_0 T_i + k_1 P_{H2O_i} + k_2 \qquad (4.14)$$

Finally, T and P_{H2O} are found when $\Delta T_i{}^u(\varphi_i)$ is equal to $\Delta T_i{}^u(T_i, P_{H2Oi})$.

Application: The 1915 Lassen Peak Volcano eruption

Plagioclase CSD and composition results

The Lassen Peak volcano is located on the southernmost Cascade Range in the Pacific coast of The United States of America. It is one of the few long-lived volcanoes which show a variable composition from andesites to rhyolites (Clynne, 1990; 1999) (Figure 4.1). Since 300 ky, a hybrid andesite consisting of mixed mafic and silicic magma has been erupted from a dacite domefield. The 1915 event was an explosive subplinian eruption that produced four volcanic rock types within 3 days: a hybrid black dacite that contains undercooled andesitic inclusions, a dark andesite and a light dacite.
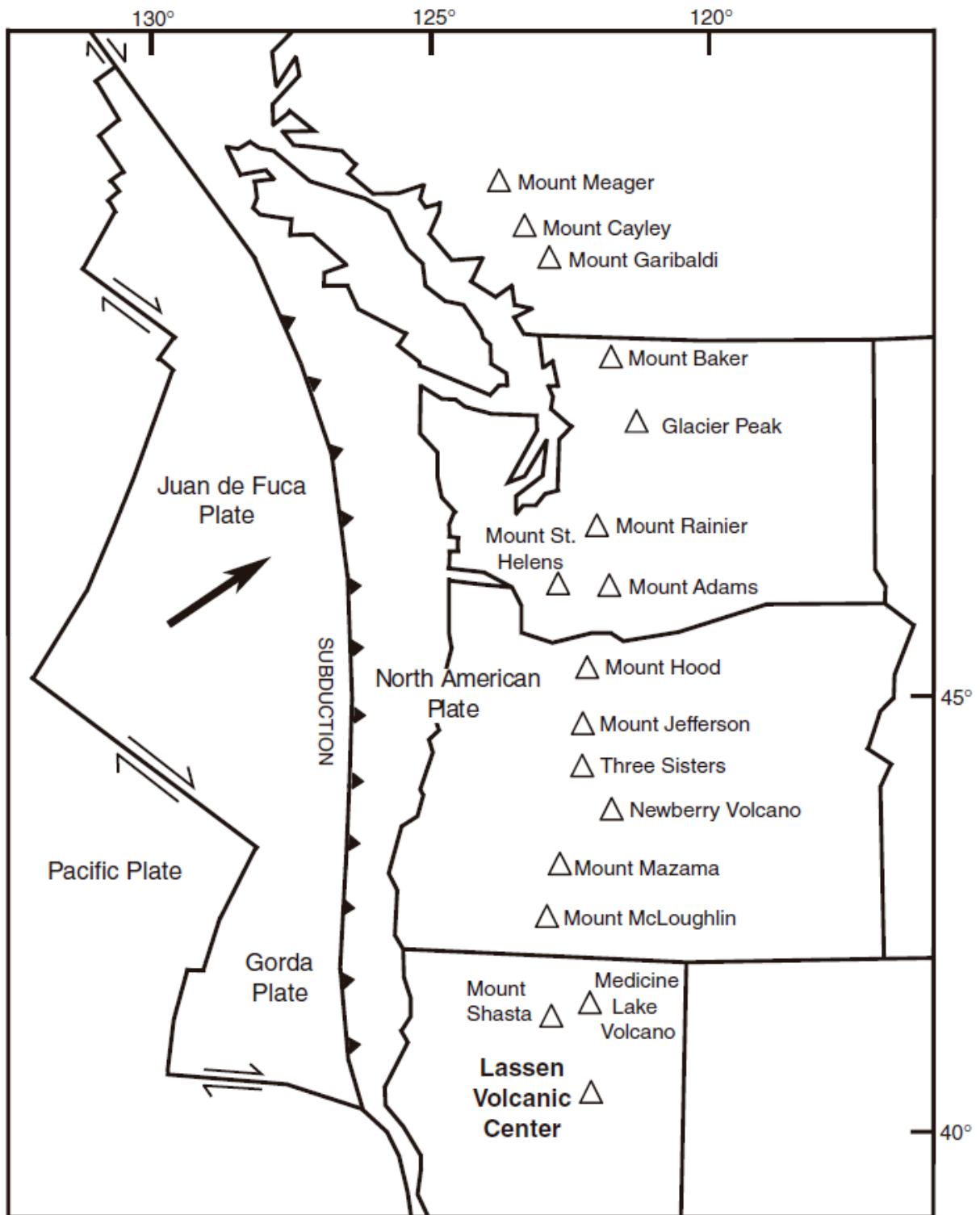
Figure 4. 1: Tectonic setting of major volcanic centers of the Cascadia subduction zone including the Lassen Peak Volcano. Extracted from Salisbury et al. (2008).

The black dacite (64 − 65 wt% SiO₂) is a coarsely porphyritic rock that contains plagioclase, biotite, hornblende and quartz phenocrysts in a microvesicular groundmass

compounded by plagioclase, clinopyroxene, orthopyroxene and titanomagnetite microcrysts. Andesitic inclusions (57 – 59.5 wt% SiO_2) contain phenocrysts of olivine and microphenocrysts of plagioclase, clinopyroxene, orthopyroxene, titanomagnetite and acicular hornblendes. The dark andesite (60 – 61 wt% SiO_2) contains olivine phenocrysts with pyroxene and plagioclase microcrysts. And the light dacite (64.5 – 68 wt% SiO_2) presents the same mineralogy of the black dacite, but with a lower volume fraction of crystals (Clynne, 1999) (Figure 4.2).
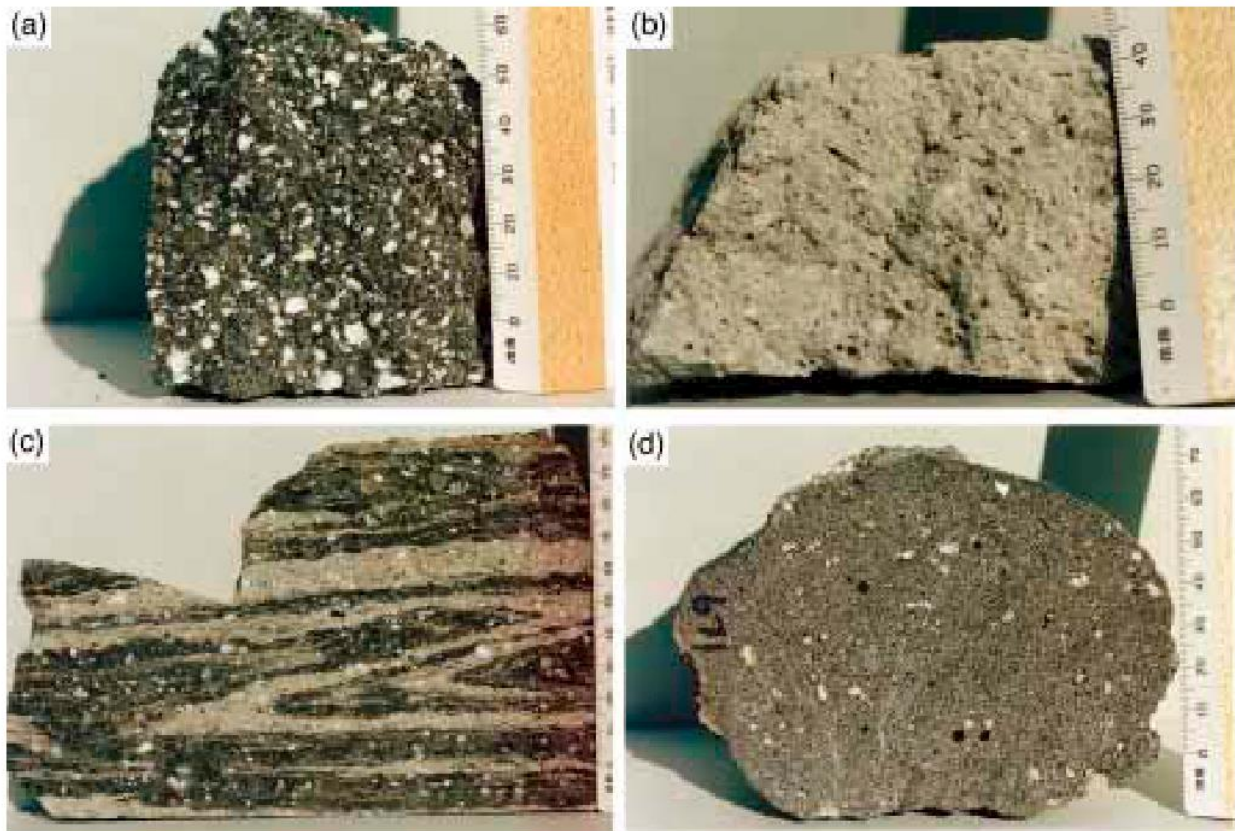
Figure 4. 2: The four kind of 1915 Lassen Peak eruption products. (a) A black dacite showing its coarsely porphyritic texture, (b) a light dacite sample showing its lower volume fraction of crystals than the black dacite, (c) a banded light dacite – dark andesite sample and (d) An andesitic inclusion sample. Extracted from Clynne, 1999.

The four kind of sample were used by Salisbury et al., (2008) to develop one plagioclase CSD analysis of every sample. In the Salisbury et al.'s work, CSDs are presented like point graphics interpolated in three linear regressions to classify phenocrysts, microphenocrysts and microlites. In our work, we interpolate the CSD data in fourth-degree polynomial regressions (Table 3.1). We do not use the dark andesite CSD because it has positive slopes. A maximum crystal length of 2.4 mm is considered

for the three CSDs according to the Salisbury et al.'s database and to the plagioclase core composition profile.

Table 4. 1: Fourth-degree polynomial regressions of the logarithm of population densities as functions of the cristal length for black dacite, light dacite and andesitic inclusión sample.

Table 4.1: Fourth-degree polynomial regressions of the logarithm of population densities as functions of the crystal length for black dacite, light dacite and andesitic inclusion sample.

	L [μm]	Ln(n(L))	L [μm]	Ln(n(L))
Black dacite	[0 - 111]	$224.37545\ L^2$ $-64.635404\ L$ 11.916179	[111 - 2400]	$1.3318817\ L^4$ $-8.6524039\ L^3$ $+20.182337\ L^2$ $-21.714101\ L$ 9.6318816
Light dacite	[0 - 647]	$135.40387\ L^4$ $-217.87838\ L^3$ $133.86656\ L^2$ $-48.740718\ L$ 11.622148	[647 - 2400]	$0.77613759\ L^2$ $-3.7810055\ L$ 2.9646677
Andesitic Inclusion	[0 - 746]	$8.2973682\ L^3$ $-17.078112\ L^2$ $-5.1741552\ L$ 9.7074493	[746 - 2400]	$-1.3268402\ L^3$ $6.3825087\ L^2$ $-10.314988\ L$ 4.4847691

The CSD of both dacites are concave curves, both present a nucleation density close to e^{12} and similar population densities between 0 and 150 μm. To higher crystal sizes, the population density of the black dacite is always higher than the population density of the light dacite with similar slopes from 600 μm to 2400 μm. The CSD of andesitic inclusions presents lower population densities than both dacite CSDs from 700 μm to 2400 μm. To crystal sizes smaller than 700 μm, the CSD is a convex curve with higher population density than both dacite CSDs and a nucleation density close to e^{10} (Figure 4.3).
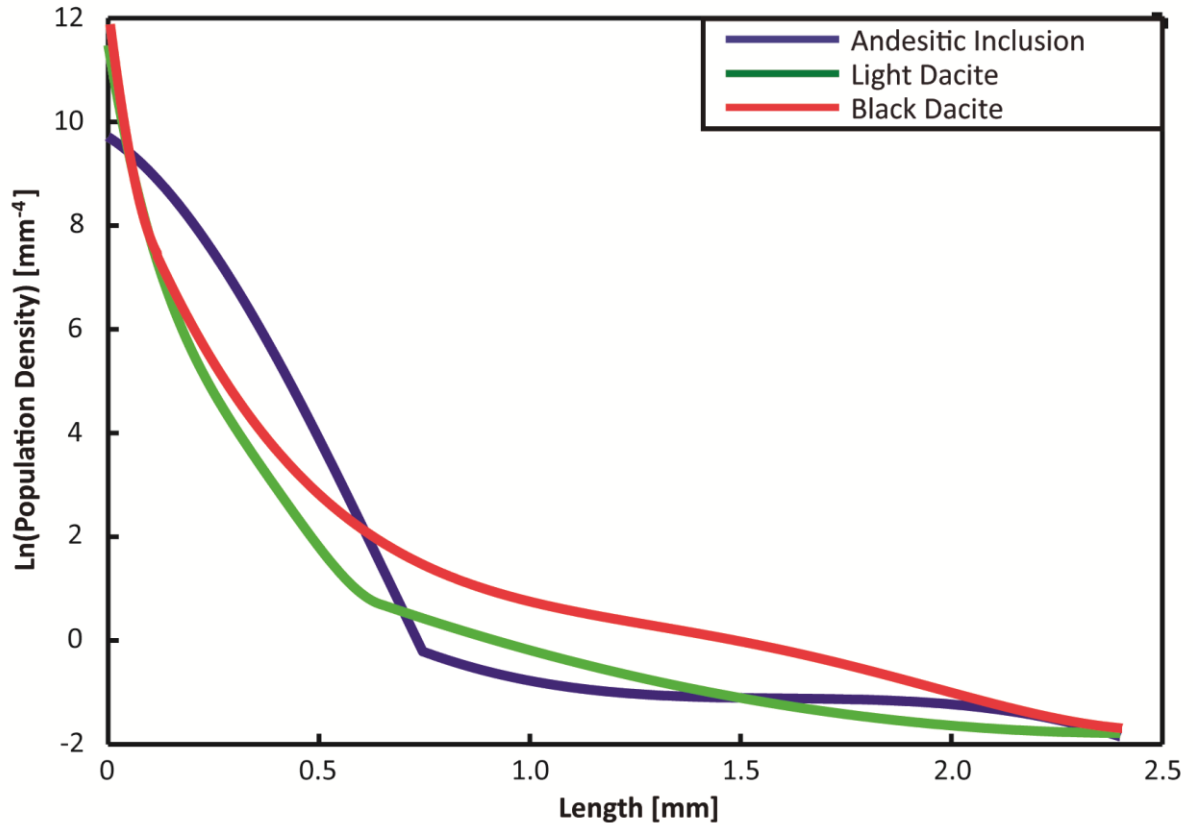
Figure 4. 3: CSDs of the three kind of samples of the 1915 Lassen Peak Volcano. A maximum crystal length of 2.4 mm is considered for the three CSD.

To calculate G, a G_M of 1 x 10^{-7} mm s^{-1} is considered for the S_M related to the first 100 μm of every CSD diagram (microlites according to the Salisbury et al.'s nomenclature) (Cashman and Blundy, 2000; Salisbury et al., 2008). Φ, J and t are calculated using equations 4.5, 4.7 and 4.8 respectively. The final φ is 0.69 of the black dacite, 0.38 of the light dacite and 1.00 of andesitic inclusions. Φ of both dacites is always higher to the φ of andesitic inclusion, but in the final crystallization stage (Figure 4.4). The calculated total duration of crystallization is 12.0 y for black dacite, 29.4 y for light dacite and 10.5 y for andesitic inclusions.
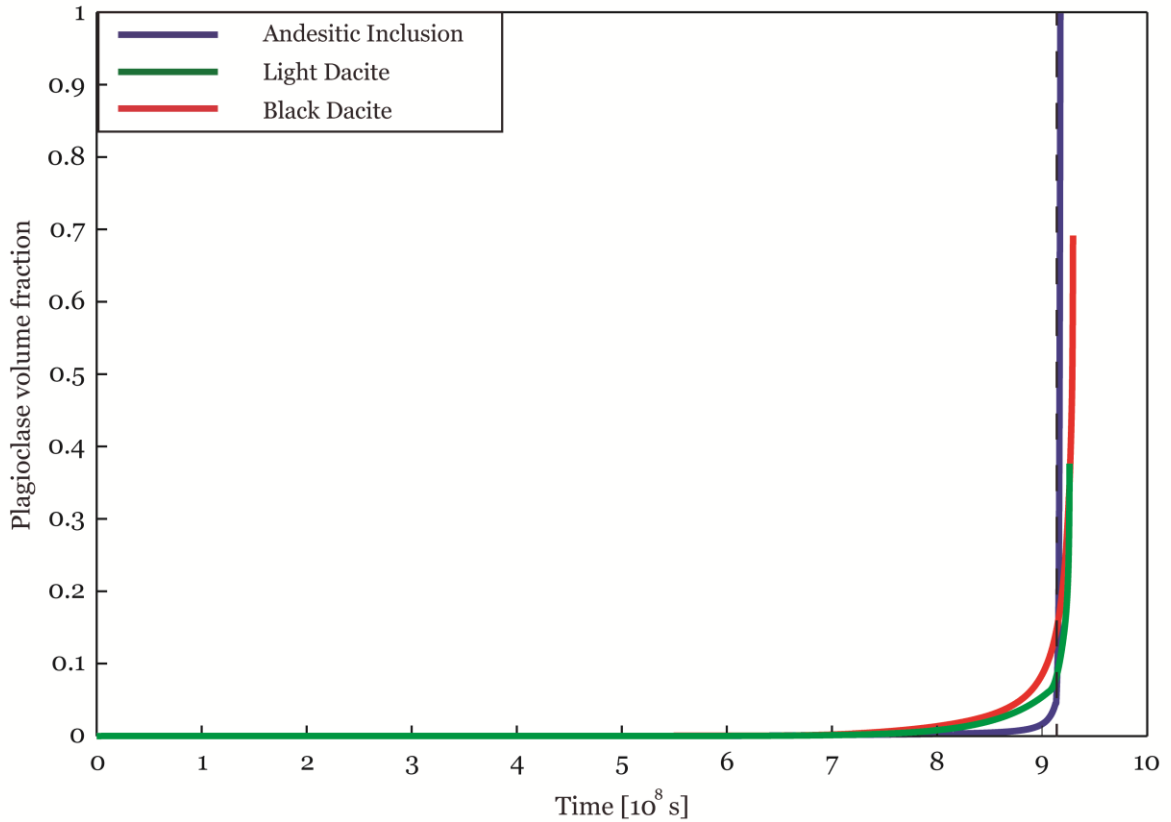
Figure 4. 4: The plagioclase crystal volume fraction for the black dacite, the light dacite and the andesitic inclusion as functions of time. The calculated final φ is 0.69, 0.38 and 1.00 respectively. Because of the different calculated duration of crystallization, the three samples do not begin in the same point; else they coincide in the inferred beginning of the eruption. Both dacites always have higher φ than the andesite, but in the last stage of crystallization.

Core and rim anorthite content profiles are presented by Salisbury et al. (2008) from 85 measured plagioclases. The rim anorthite content profile does not present a clear dependence on the crystal length (see Salisbury et al., (2008)). Consequently, we do not use this profile. The core anorthite content profile is oscillatory from 600 μm to 2400 μm with anorthite content from 0.30 to 0.44. Decreasing the crystal size, the anorthite content sharply increases up to 0.73 in only 200 μm, followed by a soft decrease up to 0.66 in 250 μm and a final sharp decrease up to 0.48 in the last 150 μm. To increase the resolution of the database, 13 plagioclase traverses were put into the core anorthite content profile (Figure 4.5). This final anorthite content profile was interpolated using fifth-degree polynomial regressions to discretize the anorthite content parameter according to our model (Table 3.2).
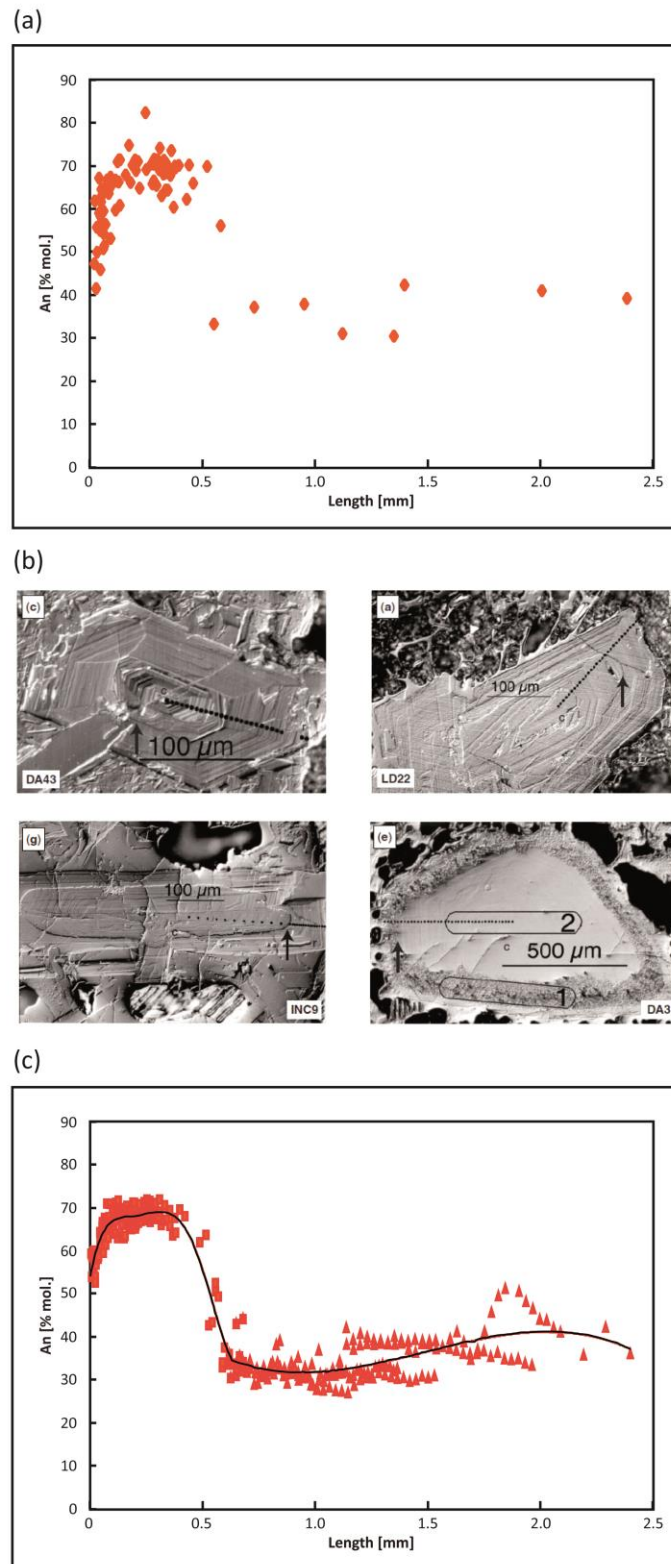
Figure 4. 5: The built anorthite content profile from Salisbury et al.'s database (2008). (a) Anorthite content core composition profile as a function of the crystal size. (b) Four of the thirteen plagioclase traverses done by Salisbury et al., (2008). (c) Traverses are input in the profile (a) to obtain a complete anorthite content profile with a higher resolution.

Table 4. 2: Fifth-degree polynomial regressions of the final anorthite content profile as a function of the crystal length.

Table 4.2: Fifth-degree polynomial regressions of the final anorthite content profile as a function of the crystal length.

| L [µm]	XAn(L)	L [µm]	XAn(L)
[0 - 618]	$96.643552\ L^5$ $-157.99516\ L^4$ $90.661176\ L^3$ $-23.764009\ L^2$ $2.9793425\ L$ 0.5338213	[618 - 2400]	$-0.1478146\ L^3$ $0.6605874\ L^2$ $-0.8533862\ L$ 0.6605860

Temperature and water pressure results

The calculation of T_l, T and P_{H2O} is done using the calculated φ according to plagioclase CSDs and using the measured anorthite content profile. Coefficients of equations 4.13 and 4.14 are taken from Cashman and Blundy (2013) that correspond to the Mount St. Helen's system considering that both volcanoes have similar whole rock composition and volcanic features. The applied coefficients from equation 1 of Cashman and Blundy (2013) have been corrected according to the Figure 10 of the same work resulting in k_0 of 5/14, k_1 of 47/399 and k_2 of -1975/7.

The model is applied in the light dacite sample because it presents the highest crystallization duration and the lowest interaction with the andesitic magma (Clynne, 1999). The anorthite content of X_{AnN} is 0.3741 and the liquidus temperature curve does not intercept this composition. For P_{H2O} between 0 and 400 MPa, the minimum undercooling to obtain plagioclase with X_{An} of 0.3741 is 87.1065 ºC, related to a crystal volume fraction of 0.2613. For this reason, we conclude that largest crystals were formed when the system already had crystals. Consequently, the initial conditions to run the model are $\varphi = 0.2613$, $\Delta T^u = 87.11$ ºC, $T_l = 916.21$ ºC, $T = 829.10$ ºC and $P_{H2O} = 199$ MPa. As this φ is different with regard to the calculated φ by CSD, the latter function is arranged to satisfy initial conditions and considering the variations in the measured anorthite content profile. As between $i = 316$ and $i = 619$ the anorthite content increases

0.35, we infer that dacitic and andesitic magmas interact in this interval. Consequently, φ is recalculated as

$$\varphi_{model} = \varphi_{CSD}, i \in [1,315] \tag{4.15}$$

$$\varphi_{model} = \varphi_{CSD} + \frac{0.2613 \times (i - 316)}{303}, i \in [316,618] \tag{4.16}$$

$$\varphi_{model} = \varphi_{CSD} + 0.2613, i \in [619,2401] \tag{4.17}$$

Finally, as the search of a $\varphi(T,P_{H2O})_i$ very close to the $\varphi(CSD)_i$ could imply high differences between a T or P_{H2O} and their following steps, a vicinity (v) for the P_{H2O} value is applied as a function of the variation in the anorthite content in the same interval such that

$$v_{i-1} = 30000 \times \left| X_{An_{i-1}} - X_{An_i} \right| \tag{4.18}$$

$$P_{H2O_{i-1}} \in \left[P_{H2O_i} - v_{i-1} ; P_{H2O_i} + v_{i-1} \right] \tag{4.19}$$

To obtain a better description and interpretation of the thermodynamic database, the record is divided in numerical stages according to inflections in the P_{H2O}. In a first stage ($i \in [2034,2401]$) with a duration of 17.8 y, P_{H2O} decreases from 199 MPa to 144 MPa, T increases from 829 °C to 858 °C and X_{An} increases from 0.37 to 0.41. Later, ($i \in [1532,2033]$) in a second period of 5.9 y, the three thermodynamic parameters returned to the initial conditions. The third stage ($i \in [687,1531]$) is characterized for a stable P_{H2O} of 199 MPa, a soft decrease on T from 829 °C to 819 °C and a soft decrease on X_{An} from 0.37 to 0.34 and a duration of 4.8 y. A fourth stage ($i \in [313,686]$) of 223 days of duration is characterized for a sharp decrease of P_{H2O} from 199 MPa to 76 MPa, a sharp increase of T from 819 °C to 959 °C and a strong increase of X_{An} from 0.34 to 0.69. In a fifth stage ($i \in [112,313]$) of 51 days of duration, P_{H2O} decreases from 76 MPa to 64 MPa and T and X_{An} are almost stable from 959 °C to 957 °C and from 0.69 to 0.67 respectively. The sixth stage lasts 7 days ($i \in [58,111]$), P_{H2O} keeps constant with 64 MPa,

T decreases from 957 ºC to 949 ºC and X_{An} decreases from 0.67 to 0.64. Finally, the seventh stage lasts 6 days (*i* ∈ [1,57]), characterized for a higher decrease of *T* from 949 ºC to 914 ºC and a higher decrease of X_{An} from 0.64 to 0.53 (Figure 4.6).

Interpretation

The 1915 Lassen Peak Volcano eruption is characterized by at least two heating events previous to the eruption, a first one of 29 ºC and a second one very higher than the former of 140ºC. Indeed, the crystallization temperature during last stages is higher than in reservoir. In both heating events, plagioclase crystals grew around 350 μm, the water pressure decreases 50 MPa and 135 MPa and X_{An} sharply increases 0.04 and 0.35 respectively. The beginning of the stage 1 and the whole stage 3 reveal the stable conditions of the dacitic reservoir of the Lassen Peak Volcano: a water pressure of 200 MPa, a temperature between 820 ºC and 830 ºC crystallizing albitic plagioclases with anorthite content from 0.34 to 0.37 and a maximum crystal size of almost 1 mm. Supposing water saturation in stable conditions and without considering the pressure of other volatiles, the depth of the dacitic reservoir is of at least 7 km that is consistent with previous studies (Guffanti and Weaver, 1988; Pitt et al., 2002). Textural features indicate that the second heating is due to an incomplete magma mixing between the dacitic and an andesitic melts (Clynne, 1999). The fifth stage shows the stable conditions after the andesite input with a water pressure between 64 MPa and 76 MPa, and X_{An} and *T* almost stables around 0.68 and 958 ºC respectively. The sixth stage would show the magma ascent stage with a decrease of *T* and X_{An} of 10 ºC and 0.03 respectively forming regrowth rims of 60 μm. Finally, the last stage show a short period of surface crystallization characterized by a decrease of 35 ºC and a variation of X_{An} from 0.64 to 0.53 forming a rim of 55 μm.
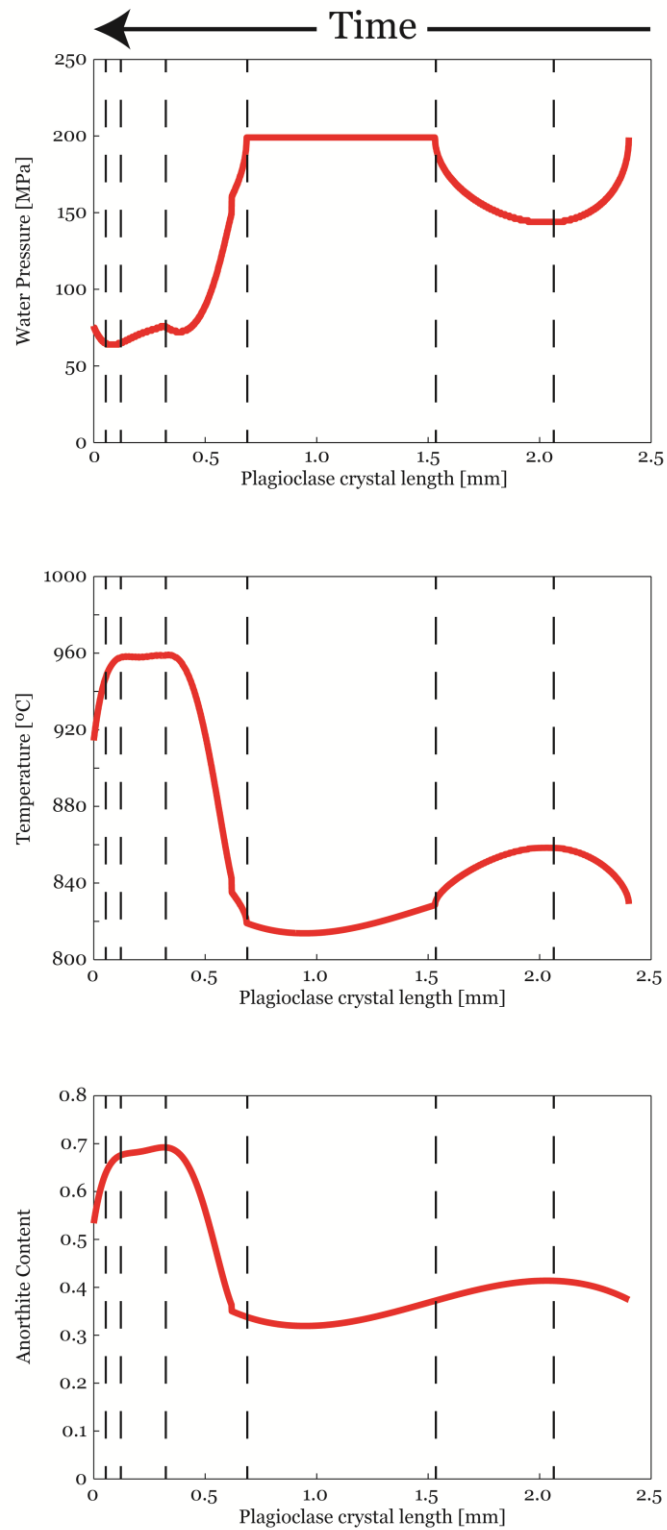
Figure 4. 6: Water pressure [MPa], Temperature [ºC] and anorthite content as functions of the plagioclase crystal length. The time advances leftward according to the applied parameterization. Dashed lines highlight the inferred magmatic stages based on inflections in the water pressure curve.
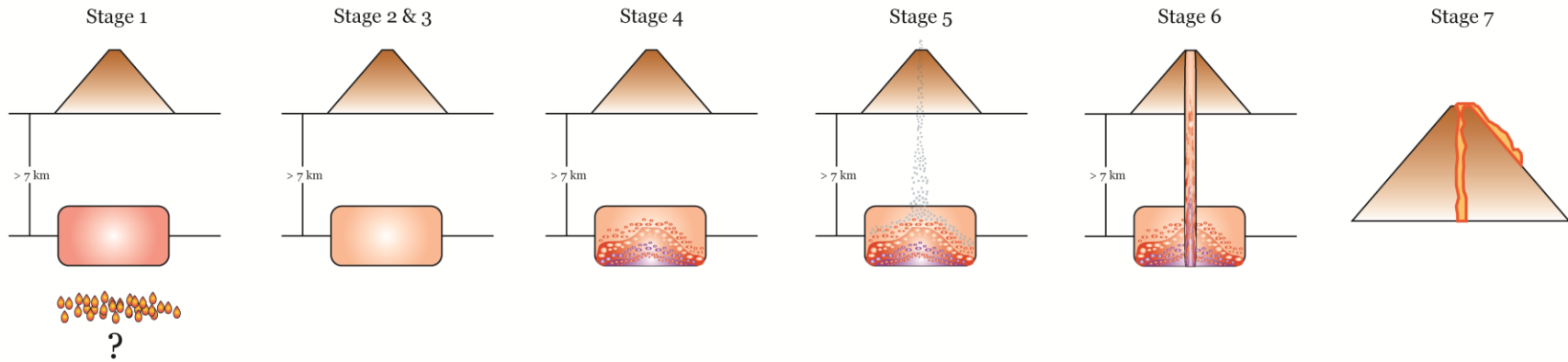
Figure 4. 7: A summary of the inferred magmatic stages for the 1915 Lassen Peak eruption. Stage 1 presents a heating of 30 ºC and a decrease of water pressure of 50 MPa, the origin of this heating is not defined. Stage 2 is the transition to stable conditions. Stage 3 lasts 0.5 y and presents almost constant temperature, water pressure and anorthite content of 829 ºC, 199 MPa and 0.37 respectively. Stage 4 represents the second event of heating with an increase of 140 ºC and decrease of water content up to 75 MPa because of the mixing between the dacitic and the andesitic magma. Stage 5 keeps the temperature and the plagioclase composition, but it shows a decrease of the water content; thus, a devolatilization is inferred. Stage 6 lasts 18 h and represents the magma ascent showing a magma ascent rate of 0.1 m s⁻¹. The stage 7 represents surface crystallization.

Considering the sixth stage as the magma ascent stage, the calculated magma ascent rate is of at least 0.01 m s^{-1} that is one order of magnitude smaller than calculated by previous studies (e.g., Rutherford, 2008). Consequently, we think that the applied mean plagioclase growth rate of 1 x 10^{-7} mm s^{-1} for plagioclase microcrysts by Salisbury et al. (2008) would be underestimated in one order of magnitude and then, the crystallization process previous to the 1915 Lassen Peak eruption would last 3 y and not 30 y. Thus, the duration of the first stage would last 1.8 y and the calculated *G* and *J* would vary from 10^{-9} mm s^{-1} to 10^{-8} mm s^{-1} and from 10$^{-9.5}$ mm^{-4} s^{-1} to 10^{-8} mm^{-4} s^{-1} which are consistent values for crystallization in reservoirs (e.g., Morgan et al., 2006). Moreover, the magma ascent and the surface crystallization stages would last 18 h and 14 h respectively which are more consistent for explosive eruptions (e.g., Rutherford, 2008) and calculated crystallization rates are around 10^{-6} mm s^{-1} for *G* and 10$^{-1.5}$ mm^{-4} s^{-1} for *J*.

Discussion

The use of plagioclase composition

Our model use the major elements of plagioclase due to several reasons: 1. Plagioclase displays a wide compositional range from basalts to rhyolites in extrusive rocks and from gabbros to granites in intrusive rocks. Consequently, our model can be used for any whole rock composition. 2. The geochemical structure of plagioclase consists in a simple binary solid solution with coupled substitution. The former feature allows the obtaining of a simple index comparable with other physical parameters and the latter index assures that major elements do not remobilize later of the closure of the system (e.g., Costa et al., 2003; Costa and Chackaborty, 2004). 3. Major elements of plagioclase are sensitive to whole rock composition, temperature and water pressure. Then, it is not needed the use of partition or diffusion coefficients or trace elements to complement our model.

The coupling of anorthite content to the calculation of crystallization rates by Crystal Size Distribution increases the resolution for deciphering magmatic stages with regard to previous semi-quantitative advances (e.g., Salisbury et al., 2008; Vinet and Higgins, 2010; 2011). For example, Salisbury et al., (2008) infer three stages based on qualitative analysis of plagioclase CSD and composition profiles and our study infer

seven. Particularly, our study allows distinguish between magma ascent and surface crystallization inside the complete syn-eruptive stage and it allows distinguish mechanical processes such as heating or magma mixing during pre-eruptive stages.

Calibration of thermodynamic constants

To use equations from 4.12 to 4.14, the thermodynamic parameters should be calibrated for different igneous systems due to the different dependence of the plagioclase composition to temperature or water content if the whole melt composition varies. A good example is the comparison between the plagioclase composition – temperature relationship shown by Schmidt et al., (2008) for primitive basalts and the plagioclase composition – temperature relationship shown by Rutherfore and Devine (2008) for dacites, both belonging to the Cascade Range. Later of the calibration, resulting crystallization temperature, liquidus temperature and water pressure are output as functions of the plagioclase crystal size and the time due to the parallel CSD analysis, allowing showing the evolution of thermodynamic parameters and easing the exhibition of a sequentially interpretation of magmatic processes. The water pressure can be easily converted to water content using numerical thermodynamic softwares (e.g., Newman and Lowenstern, 2002).

Analytical errors

The analytical errors of our coupled model can be divided from its two sources: error from the CSD analysis and error from the thermodynamic acquirement. The former presents two main sources of error: 1. The counting error related to potential differences between measurements of a same crystal that is more significant for crystal sizes with smaller population densities and 2. The related error to the method used to the stereological conversion.

The thermodynamic procedure presents X main sources of error: 1. The analytical error related to the acquisition of plagioclase composition. 2. The r^2 belonging to the polynomial regressions to create the final anorthite content profile. 3. The related error to the numerical method to calibrate the thermodynamic coefficients.

Conclusion

The presented model combines the Crystal Size Distribution analysis with the anorthite content in plagioclase to constrain magmatic processes with a higher resolution than using only quantitative textural analysis. Crystal Size Distributions allow calculate crystallization kinetic parameter as functions of the crystal size and the anorthite content is intrinsically a function of the crystal size.

Previous works have shown that as crystal kinetic parameters such as the crystal growth rate, the crystal nucleation rate and the volume fraction of crystals as the plagioclase composition are functions of thermodynamic parameters such as the temperature and the water pressure (e.g., Spohn et al., 1988; Hort, 1997; Rutherford and Devine, 2008). Thus, both thermodynamic parameters can be calculated as functions of the crystal size through the calculation of kinetic parameters by CSD and the measurement of the anorthite content in plagioclase.

The presented model was applied in the volcanic products of the 1915 Lassen Peak volcano eruption giving one heating process followed by a stable stage of the dacitic reservoir that show P_{H2O} of 200 MPa, T of 830 ºC forming plagioclase of X_{An} = 0.37. The stable stage is followed by a strong heating due to a magma mixing between the dacitic magma and an andesitic magma that changes the thermodynamic conditions to P_{H2O} of 76 MPa, T of 959 ºC forming plagioclase of X_{An} = 0.68. The eruption is preceded by a short stage of devolatilization and followed by a surface crystallization stage. As a summary, a record of seven stages is measured due to the coupling of CSD analysis and plagioclase composition.

Secondarily, as the water pressure is constant during the stable stage, water saturation is assumed giving a minimum depth of the dacitic reservoir of 7 km. The magma ascent lasts 18 hours according to the CSD calculation implying a magma ascent rate of 0.1 m s^{-1}.

Capítulo 5

Resumen y conclusiones

El presente trabajo ha presentado el diagnóstico de diversos problemas en el procedimiento para realizar análisis *Crystal Size Distributions*: 1. Convencionalmente, se parametriza el eje de tamaño de cristal usando una distribución logarítmica siendo que la densidad de población de cristales es la derivada de la distribución acumulada de tamaños de cristales, la que es una función continua y derivable, por lo tanto, no necesita ser discretizada, 2. Se realiza una conversión estereológica de los datos en 2 dimensiones para convertirlos a datos en 3 dimensiones suponiendo que todos los cristales presentan la misma razón de aspecto y que cumplen funciones probabilísticas de corte; no obstante, la razón de aspecto es función del *undercooling* y de la tasa de enfriamiento y empíricamente, los cristales en rocas ígneas no siguen tendencias ordenadas. 3. Las tasas de nucleación y crecimiento de cristales calculadas a partir de CSD con los modelos de *Open System*, *Batch System* o inversión de CSD entregan ambas tasas constantes, tasa de crecimiento constante y tasa de nucleación crecientemente exponencial o tasa de crecimiento decrecientemente exponencial y tasa de nucleación crecientemente exponencial con respecto al tiempo respectivamente; no obstante, las tasas de crecimiento y nucleación calculadas numérica y experimentalmente considerando la energía de activación necesaria para nuclear y crecer presentan distribuciones con forma de campana y asimétricas, encontrándose el pico de la tasa de crecimiento siempre previo al de nucleación.

Para solucionar este problema, se ha creado un modelo de obtención de diagramas de CSD basado en el análisis de la curva de distribución acumulada de tamaños de cristales, usando los tamaños de largo y área medidos en 2 dimensiones, entendiendo la curva como una función continua y derivable. Por lo tanto, se utiliza una función error para modelarla. El CSD obtenido es corregido desplazando la densidad de población de cristales tal que la fracción volumétrica de cristales calculada sea igual a la fracción de área de cristales medida. El resultado es un CSD convexo el cual es parametrizado para la aplicación de un modelo de inversión de CSD para el cálculo de tasas de crecimiento y nucleación entendiendo que los cristales más largos son más

antiguos (por lo tanto, el eje tiempo avanza hacia la izquierda en un CSD) y que la tasa de crecimiento es proporcional al negativo de la pendiente del CSD. Las tasas de crecimiento y nucleación de cristales obtenidos presentan curvas de distribución gaussiana asimétricas con respecto al tiempo, encontrándose siempre el pico de la tasa de crecimiento previo al de la tasa de nucleación tal como registran modelos numéricos y experimentales y la fracción volumétrica de cristales presenta curvas sigmoidales tal como modelos numéricos y experimentales lo han presentado.

Este modelo fue aplicado en un sistema ígneo extrusivo y en un sistema ígneo intrusivo: lavas de 1971 del Volcán Villarrica y cuarzo-monzodioritas del Plutón La Gloria, respectivamente. En el primer caso, se entrega un CSD con un *kink*, que separa microlitos de fenocristales, ubicado en una posición coherente con lo observado texturalmente cualitativamente. Los diagramas de ambas tasas de cristalización con respecto al tiempo muestran claramente como una erupción, como evento instantáneo, aumenta la tasa de crecimiento en dos órdenes de magnitud y la de nucleación en 8 órdenes de magnitud y como la fracción volumétrica de cristales se duplica en la fase syn-eruptiva respecto a la fase pre-eruptiva. Los tiempos calculados son de 7 años para la fase pre-eruptiva y 17 días para la fase syn-eruptiva. El primer tiempo coincide con el desfase entre esta y su erupción previa (1964) dejando abierta la hipótesis de contener cristales heredados del ciclo eruptivo anterior. El segundo tiempo es alto para corresponder únicamente a ascenso y cristalización en superficie.

En el segundo caso, se entrega un CSD convexo ya que se consideró cristalización continua. Este ejemplo ilustra muy bien las distribuciones gaussianas asimétricas de ambas tasas de cristalización y una distribución sigmoidal de la fracción volumétrica de cristales con respecto al tiempo. Esta última curva es dividida en 3 etapas según sus inflexiones: 1. Una etapa de muy bajo incremento de la fracción volumétrica de cristales la que coincide con el pico de la tasa de crecimiento lo que evidencia que al no considerarse antecristales, el aumento de la fracción volumétrica es lento, 2. Una etapa de crecimiento muy fuerte de la fracción volumétrica de cristales que coincide con el pico de la tasa de nucleación de cristales evidenciando la mayor dependencia de la fracción volumétrica a la nucleación que al crecimiento de cristales, 3. Un descenso en el incremento de la fracción volumétrica de cristales debido a la disminución del espacio disponible para nuclear nuevos cristales o para recrecer los antiguos.

Luego de la obtención de tasas de crecimiento y nucleación y de la fracción volumétrica de cristales similares a los esperables, el CSD seguiría sin poder distinguir procesos magmáticos con una alta resolución, por ejemplo: no distingue entre la fase de ascenso de magma y la de cristalización en superficie dentro de la fase syn-eruptiva; o no distingue procesos mecánicos en reservorio tales como mezcla de magma o cristalización en multireservorios para la fase pre-eruptiva.

Basado en que tanto los parámetros cinéticos de cristalización como el contenido de anortita en plagioclasa son función de la temperatura y de la presión de agua estos últimos pueden ser calculados si se cuenta con los primeros. Para esto se utiliza la relación de la fracción volumétrica de cristales con el *undercooling*, la temperatura *liquidus* se expresa como un polinomio de la presión de agua y el contenido de anortita como función de lineal de la temperatura y de la presión de agua.

Estas bases numéricas son aplicadas para la erupción de 1915 del Volcán Lassen ubicado en la Cordillera Cascadia ubicada en la costa oeste de Estados Unidos utilizando los CSDs y el perfil del contenido de anortita en plagioclasa desarrollado por Morgan Salisbury y colaboradores (2008). Los resultados entregan que se requiere de una fracción volumétrica de cristales mínima de 0.26 al inicio del proceso. Se registran dos procesos de calentamiento previos a la erupción: el primero de 30 °C y el segundo de 140 °C. Además, existe una fase muy estable previa al segundo calentamiento que registra una presión de agua de 200 MPa, una temperatura de 830 °C generando plagioclasas con contenido de anortita de 0.37. Dada la estabilidad y suponiendo que el agua no es el único volátil que se encuentra en el sistema, se entiende saturación del agua y, por ende, presión litostática igual a presión de fluidos. En consecuencia, se fija una cota mínima de 200 MPa de presión litostática del reservorio dacítico correspondiente a unos 7 km de profundidad, resultado coherente a estudios previos. Posterior al segundo calentamiento, la temperatura se estabiliza, pero la presión de agua disminuye por lo que se interpreta como una fase de desvolatilización justo previa a la erupción. Se calcula un ascenso magmático de 18 horas, lo que correspondería a una tasa de ascenso magmático mínima de aproximadamente 0.11 m s^{-1}, resultado coherente con erupciones explosivas dacíticas. El tiempo total del proceso de cristalización registrado son aproximadamente, 3 años.

La aplicación de nuestro modelo confirma que el acoplamiento del cálculo de parámetros cinéticos de cristalización con la composición de los mismos minerales permite la obtención de una evolución petrológica de sistemas magmáticos de gran resolución con que es posible distinguir procesos magmáticos pre-eruptivos tales como calentamiento, mezcla de magma y devolatilización y es posible distinguir procesos magmáticos syn-eruptivos tales como ascenso de magma y cristalización en superficie.

Bibliografía

Albarede, F. (1993). Residence time analysis of geochemical fluctuations in volcanic series. *Geochimica et Cosmochimica* Acta **57**, 615-621.

Allègre, C. J., Provost, A. & Jaupart, C. (1981). Oscillatory zoning: a pathological case of cristal growth. *Nature* **294**, 223–228.

Armienti, P., Francalanci, L. & Landi, P. (2007). Textural effects of steady state behaviour of the Stromboli feeding system. *Journal of Volcanology and Geothermal Research* **160**, 86–98.

Armienti, P., Pareschi, M. T., Innocenti, F. & Pompilio, M. (1994). Effects of magma storage and ascent on the kinetics of cristal growth. The case of the 1991-93 Mt. Etna eruption. *Contributions to Mineralogy and Petrology* **115**, 402–414.

Avrami, M. (1939). Kinetics of phase change I. General theory. *Journal of Chemical Physics* **7**, 1103–1112.

Avrami, M. (1940). Kinetics of phase change II. Transformation-time relation for random distribution of nuclei. *Journal of Chemical Physics* **8**, 211–224.

Bachmann, O & Bergantz, G. W. (2004). On the origin of crystal-poor rhyolites: extracted from batholitic crystal mushes. *Journal of Petrology* **45**, 1565–1582.

Blundy, J. & Cashman, K. V. (2005). Rapid decompression-driven crystallization recorded by melt inclusions from Mount St. Helens volcano. *Geology* **33**, 793-796.

Blundy, J., Cashman, K., Humphreys, M. (2006). Magma heating by decompression-driven crystallization beneath andesite volcanoes. *Nature* **443**, 76–80.

Bouvet de Maisonneuve, C., Dungan, M. A., Bachmann, O. & Burgisser, A. (2012). Insights into shallow magma storage and crystallization at Volcán Llaima (Andean Southern Volcanic Zone, Chile). *Journal of Volcanology and Geothermal Research* **211-212**, 76–91.

Bouvet de Maisonneuve, C., Dungan, M. A., Bachmann, O. & Burgisser, A. (2013). Petrological insights into shifts in eruptive styles at Volcán Llaima (Chile). *Journal of Petrology* **54**, 393–420.

Bowen, N. L. (1913). The melting phenomena of the plagioclase feldspars. *American Journal of Science* **35**, 577-599.

Cashman, K. & Blundy, J. (2013). Petrological cannibalism: the chemical and textural consequences of incremental magma body growth. *Contributions to Mineralogy and Petrology* **166**, 703–729.

Cashman, K. V. (1992). Groundmass crystallization of Mount St. Helens dacite, 1980 – 1986: a tool for interpreting shallow magmatic processes. *Contributions to Mineralogy and Petrology* **109**, 431–449.

Cashman, K. V. (1993). Relationship between plagioclase crystallization and cooling rate in basaltic melts. *Contributions to Mineralogy and Petrology* **113**, 126–142.

Cashman, K. V., Thornber, C. & Kauahikaua, J. P. (1999). Cooling and crystallization of lava in open channels, and the transition of Pahoehoe Lava to 'A'a. *Bulletin of Volcanology* **61**, 306-323.

Cashman, K. V. & Blundy, J. (2000). Degassing and crystallization of ascending andesite and dacite. *Philosophical Transactions of the Royal Society of London* **358**, 1487-1513.

Cashman, K. V. & Marsh, B. D. (1988). Crystal size distribution (CSD) in rocks and the kinetics and dynamics of crystallization II: Makaopuhi lava lake. *Contributions to Mineralogy and Petrology* **99**, 292–305.

Clynne, M. A. (1990). Stratigraphic, lithologic, and major element geochemical constraints on magmatic evolution at Lassen volcanic center, California. *Journal of Geophysical Research* **95**, 19651-19669.

Clynne, M. A. (1999). A complex magma mixing origin for rocks erupted in 1915, Lassen Peak, California. *Journal of Petrology* **40**, 105-132.

Condomines, M., Hemond, C. & Allegre, C. J. (1988). U–Th–Ra radioactive disequilibria and magmatic processes. *Earth and Planetary Science Letters* **90**, 243–262.

Cornejo, P. C. & Mahood, G. A. (1997). Seeing past the effects of re-equilibration to reconstruct magmatic gradients in plutons: La Gloria Pluton, central Chilean Andes. *Contributions to Mineralogy and Petrology* **127**, 159–175.

Costa, F. & Chakraborty, S. (2004). Decadal time gaps between mafic intrusion and silicic eruption obtained from chemical zoning patterns in olivine. *Earth and Planetary Science Letters* **227**, 517-530.

Costa, F., Chakraborty, S. & Dohmen, R. (2003). Diffusion coupling between trace and major elements and a model for calculation of magma residence times using plagioclase. *Geochimica et Cosmochimica Acta* **67**, 2189-2200.

Couch, S., Sparks, R. S. J. & Carroll, M. R. (2003). The kinetics of degassing-induced crystallization at Soufriere Hills Volcano, Montserrat. *Journal of Petrology* **44**, 1477-1502.

Crisp, J., Cashman, K. V., Bonini, J. A., Hougen, S. B. & Pieri, D. C. (1994). Crystallization history of the 1984 Mauna Loa lava flow. *Journal of Geophysical Research* **99**, 7177-7198.

Davidson, J., Tepley, F., Palacz, Z. & Meffan-Main, S. (2001). Magma recharge, contamination and residence times revealed by in situ laser ablation isotopic analysis of feldspar in volcanic rocks. *Earth and Planetary Science Letters* **184**, 427-442.

Eberl, D. D., Drits, V. A. & Srodon, J. (1998). Deducing growth mechanisms for minerals from the shapes of crystal sizes distributions. *American Journal of Science* **298**, 499–533.

Eberl, D. D., Kile, D. E. & Drits, V. A. (2002). On geological interpretations of crystal size distributions: Constant vs proportionate growth. *American Mineralogist* **87**, 1235–1241.

Ernst, R. E., Fowler, A. D. & Pearce, T. H. (1988). Modelling of igneous fractionation and other processes using Pearce diagrams. *Contributions to Mineralogy and Petrology* **100**, 12–18.

Ghiorso, M. S. & Sack, R. O. (1995). Chemical mass transfer in magmatic processes IV, A revised and internally consistent thermodynamic model for the interpolation and extrapolation of liquid-solid equilibria in magmatic systems at elevated temperatures and pressures. *Contributions to Mineralogy and Petrology* **119**, 197–212.

Gorokhova, N. V. & Melnik, O. E. (2010). Modeling of the Dynamics of Diffusion Crystal Growth from a Cooling Magmatic Melt. *Fluid Dynamics* **45**, 679–690.

Guffanti, M. & Weaver, C. S. (1988). Distribution of Late Cenozoic Volcanic Vents in the Cascade Range: Volcanic Arc Segmentation and Regional Tectonic Considerations. *Journal of Geophysical Research* **93**, 6513–6529.

Gutierrez, F., Payacan, I., Gelman, S. E., Bachmann, O. & Parada, M. A. (2013). Late-stage magma flow in a shallow felsic reservoir: merging the anisotropy of magnetic susceptibility record with numerical simulations in La Gloria Pluton, central Chile. *Journal of Geophysical Research* **118**, 1984–1998.

Hammer, J. E., Cashman, K. V., Hoblitt, R. P. & Newman, S. (1999). Degassing and microlite crystallization during pre-climactic events of the 1991 eruption of Mt. Pinatubo, Philippines. *Bulletin of Volcanology* **60**, 355-380.

Hawkesworth, C. J., Blake, S., Evans, P., Hughes, R., Macdonald, R., Thomas, L. E., Turner, S. P. & Zellmer, G. (2000). Time Scales of Crystal Fractionation in Magma Chambers – Integrating Physical, Isotopic and Geochemical Perspectives. *Journal of Petrology* **41**, 991-1006.

Hawkesworth, C., George, R., Turner, S. & Zellmer, G. (2004). Time scales of magmatic processes. *Earth and Planetary Science Letters* **218**, 1-16.

Higgins, M. D. (1996). Magma dynamics beneath Kameni volcano, Greece, as revealed by crystal size and shape measurements. *Journal of Volcanology and Geothermal Research* **70**, 37–48.

Higgins, M. D. (2000). Measurements of crystal size distributions. *American Mineralogist* **85**, 1105–1116.

Higgins, M. D. (2002a). Closure in crystal size distributions (CSD), verification of CSD calculations, and the significance of CSD fans. *American Mineralogist* **87**, 171–175.

Higgins, M. D. (2002b). A crystal size-distribution study of the Kiglapait layered mafic intrusion, Labrador, Canada: evidence for textural coarsening. *Contributions to Mineralogy and Petrology* **144**, 314–330.

Higgins, M. D. (2006). *Quantitative Textural Measurements in Igneous and Metamorphic Petrology*. Cambridge University Press, 265 pp.

Higgins, M. D. & Roberge, J. (2003). Crystal Size Distribution of Plagioclase and Amphibole from Soufrière Hills Volcano, Montserrat: Evidence for Dynamic Crystallization-Textural Coarsening Cycles. *Journal of Petrology* **44**, 1401–1411.

Holland, T. & Powell, R. (2003). Activity-composition relations for phases in petrological calculations: an asymmetric multicomponent formulation. *Contributions to Mineralogy and Petrology* **145**, 492–501.

Hort, M. (1997). Cooling and crystallization in sheet-like magma bodies revisited. *Journal of Volcanology and Geothermal Research* **76**, 297–317.

Hort, M. & Spohn, T. (1991). Crystallization calculations for a binary melt cooling at constant rates of heat removal: implications for the crystallization of magma bodies. *Earth and Planetary Science Letters* **107**, 463–474.

Jerram, D. A., Cheadle, M. J., Hunter, R. H. & Elliott, M. T. (1996). The spatial distribution of grains and crystals in rocks. *Contributions to Mineralogy and Petrology* **125**, 60–74.

Jerram, D. A. & Higgins, M. D. (2007). 3D Analysis of rock textures: Quantifying igneous microstructures. *Elements* **3**, 239–245.

Kirkpatrick, J. R. (1976). Towards a kinetic model for the crystallization of magma bodies. *Journal of geophysical research* **81**, 2565–2571.

Kirkpatrick, R. J., Klein, L., Uhlmann, D. R. & Hays, J. F. (1979). Rates and Processes of crystal growth in the system Anorthite-Albite. *Journal of Geophysical Research* **84**, 3671–3676.

Lange, R. A., Frey, H. M. & Hector, J. (2009). A thermodynamic model for the plagioclase-liquid hygrometer/thermometer. *American Mineralogist* **94**, 494–506.

Lasaga, A. C. (1982). Toward a master equation in crystal growth. *American Journal of Science* **282**, 1264–1288.

L'Heureux, I. (1993). Oscillatory zoning in crystal growth: A constitutional undercooling mechanism. *Physical Review E.* **48**, 4460–4469.

L'Heureux, I. & Fowler, A. D. (1996). Dynamical model of oscillatory zoning in plagioclase with nonlinear partition relation. *Geophysical Research Letters* **23**, 17–20.

Lofgren, G. E. (1974). An experimental study of plagioclase crystal morphology: isothermal crystallization. *American Journal of Science* **274**, 243–273.

Lohmar, S., Parada, M., Gutierrez, F., Robin, C. & Gerbe, M. C. (2012). Mineralogical and numerical approaches to establish the pre-eruptive conditions of the mafic Licán Ignimbrite, Villarrica Volcano (Chilean Southern Andes). *Journal of Volcanology and Geothermal Research* **235-236**, 55–69.

Maaloe, S., Tumyr, O. & James, D. (1989). Population density and zoning of olivine phenocrysts in tholeiites from Kauai, Hawaii. *Contributions to Mineralogy and Petrology* **101**, 176–186.

Marsh, B. D. (1981). On the crystallinity, probability of occurrence, and rheology of lava and Magma. *Contributions to Mineralogy and Petrology* **78**, 85–98.

Marsh, B. D. (1988). Crystal size distribution (CSD) in rocks and the kinetics and dynamics of crystallization I: Theory. *Contributions to Mineralogy and Petrology* **99**, 277–291.

Marsh, B. D. (1996). Solidification fronts and magmatic evolution. *Mineralogical Magazine* **60**, 5–40.

Marsh, B. D. (1998). On the Interpretations of Crystal Size Distributions in Magmatic Systems. *Journal of Petrology* **39**, 553–599.

Mastrolorenzo, G. & Pappalardo, L. (2006). Magma degassing and crystallization processes during eruptions of high-risk Neapolitan-volcanoes: Evidence of common equilibrium rising processes in alkaline magmas. *Earth and Planetary Science Letters* **250**, 164–181.

Melnik, O. E., Blundy, J. D., Rust, A. C. & Muir, D. D. (2011). Subvolcanic plumbing systems imaged through crystal size distributions. *Geology* **39**, 403–406.

Mock, A. & Jerram, D. A. (2005). Crystal Size Distributions (CSD) in three dimensions: Insights from the 3D reconstruction of a highly porphyritic rhyolite. *Journal of Petrology* **46**, 1525–1541.

Moitra, P., Gonnermann, H. M., Houghton, B. F. & Giachetti, T. (2013). Relating vesicle shapes in pyroclasts to eruption styles. *Bulletin of Volcanology* **75**, 691-704.

Moreno, H. & Clavero, J. (2006). Geología del volcán Villarrica, Regiones de La Araucanía y de Los Lagos. Servicio Nacional de Geología y Minería, Carta Geológica de Chile, Serie Geología Básica, No. 98, 35 pp.

Morgan, D. J. & Blake, S. (2006). Magmatic residence times of zoned phenocrysts: introduction and application of the binary element diffusion modeling (BEDM) technique. *Contributions to Mineralogy and Petrology* **151**, 58–70.

Morgan, D. J., Blake, S., Rogers, N. W., DeVivo, B., Rolandi, G., Macdonald, R. & Hawkesworth, C. J. (2004). Time scales of crystal residence and magma chamber volume from modelling of diffusion profiles in phenocrysts: Vesuvius 1944. *Earth and Planetary Science Letters* **222**, 933–946.

Morgan, D. J. & Jerram, D. A. (2006). On estimating crystal shape for crystal size distribution analysis. *Journal of Volcanology and Geothermal Research* **154**, 1-7.

Mujin, M. & Nakamura, M. (2014). A nanolite record of eruption style transition. *Geology* **42**, 611–614.

Muncill, G. E. & Lasaga, A. C. (1987). Crystal-growth kinetics of plagioclase in igneous system: One-atmosphere experiments and applications of a simplified growth model. *American Mineralogist* **72**, 299–311.

Murphy, M. D., Sparks, R. S. J., Barclay, J., Carroll, M. R. & Brewer, T. S. (2000). Remobilization of andesite magma by intrusion of mafic magma at the Soufriere Hills Volcano, Montserrat, West Indies. *Journal of Petrology* **54**, 393–420.

Newman, S. & Lowenstern, J. B. (2002). VOLATILECALC: a silicate melt-H2O-CO2 solution model written in Visual Basic for Excel. *Computers and Geosciences* **28**, 597-604.

Noguchi, S., Toramaru, A. & Nakada, S. (2008). Relation between microlite textures and discharge rate during the 1991–1995 eruptions at Unzen, Japan. *Journal of Volcanology and Geothermal Research* **175**, 141–155.

Pappalardo, L. & Mastrolorenzo, G. (2010). Short residence times for alkaline Vesuvius magmas in a multi-depth supply system: Evidence from geochemical and textural studies. *Earth and Planetary Science Letters* **296**, 133-143.

Pitt, A. M., Hill, D. P., Walter, S. W. & Johnson, M. J. S. (2002). Midcrustal, Long-period Earthquakes beneath Northern California Volcanic Areas. *Seismological Research Letters* **73**, 144–152.

Preece, K., Barclay, J., Gertisser, R. & Herd, R. A. (2013). Textural and micro-petrological variations in the eruptive products of the 2006 dome-forming eruption of Merapi volcano, Indonesia: Implications for sub-surface processes. *Journal of Volcanology and Geothermal Research* **261**, 98–120.

Pupier, E., Duchene, S. & Toplis, M. J. (2008). Experimental quantification of plagioclase crystal size distribution during cooling of a basaltic liquid. *Contributions to Mineralogy and Petrology* **155**, 555–570.

Putirka, K. D. (2008). Thermometers and Barometers for Volcanic Systems. *Reviews in Mineralogy & Geochemistry* **69**, 61–120.

Randolph, A. D. & Larson, M. A. (1971). *Theory of particulate processes*. Academic Press, New York, 251 pp.

Resmini, R. G. (2007). Modeling of crystal size distributions (CSDs) in sills. *Journal of Volcanology and Geothermal Research* **161**, 118–130.

Riker, J. M., Cashman, K. V., Kauahikaua, J. P. & Montierth, C. M. (2009). The length of channelized lava flows: Insight from the 1859 eruption of Mauna Loa Volcano, Hawai'i. *Journal of Volcanology and Geothermal Research* **183**, 139–156.

Royet, J. P. (1991). Stereology: A method for analyzing images. *Progress in Neurobiology* **37**, 433–474.

Rutherford, M. J. (2008). Magma Ascent Rates. *Reviews in Mineralogy and Geochemistry* **69**, 241–271.

Rutherford, M. J. & Devine, J. D. (2008). *Magmatic conditions and processes in the storage zone of the 2004–2006 Mount St. Helens Dacite*. In Sherrod DR, Scott WE, Stauffer PH (eds) A volcano rekindled; the renewed eruption of Mount St. Helens, 2004–2006. U.S. Geological Survey Professional Paper **1750**, 703–726

Sahagian, D. L. & Proussevitch, A. A. (1998). 3D particle size distributions from 2D observations; stereology for natural applications. *Journal of Volcanology and Geothermal Research* **84**, 173–196.

Salisbury, M. J., Bohrson, W. A., Clynne, M. A., Ramos, F. C. & Hoskin, P. (2008). Multiple plagioclase crystal populations identified by crystal size distribution and in situ chemical data: Implications for timescales of magma chamber processes associated with the 1915 eruption of Lassen Peak, CA. *Journal of Petrology* **49**, 1755–1780.

Saltikov, S. A. (1967). The determination of the size distribution of particles in an opaque material from a measurement of the size distributions of their sections. In H. Elias, ed., *Proceedings of the Second International Congress for Stereology*. Berlin: Springer-Verlag, pp. 163–173.

Schmidt, M. E., Grunder, A. L. & Rowe, M. C. (2008). Segmentation of the cascade arc as indicated by Sr and Nd isotopic variation among diverse primitive basalts. *Earth and Planetary Science Letters* **266**, 166–181.

Sharp, T. G., Stevenson, R. J. & Dingwell, D. B. (1996). Microlites and "nanolites" in rhyolitic glass: microstructural and chemical characterization. *Bulletin of Volcanology* **57**, 631–640.

Shea, T. & Hammer, J. E. (2013). Kinetics of cooling- and decompression-induced crystallization in hydrous mafic-intermediate magmas. *Journal of Volcanology and Geothermal Research* **260**, 127-145.

Shea, T., Houghton, B. F., Gurioli, L., Cashman, K. V., Hammer, J. E. & Hobden, B. J. (2010). Textural studies of vesicles in volcanic rocks: An integrated methodology. *Journal of Volcanology and Geothermal Research* **190**, 271–289.

Sigmarsson, O., Chmeleff, J., Morris, J. & Lopez-Escobar, L. (2002). Origin of 226Ra-230Th disequilibria in arc lavas from southern Chile and implications for magma transfer time. *Earth and Planetary Science Letters* **196**, 189–196.

Smith, J. V. (1972). Critical Review of synthesis and occurrence of plagioclase feldspars and a possible phase diagram. *Geology* **80**, 505-525.

Spillar, V. & Dolejs, D. (2013). Calculation of Time-dependent Nucleation and Growth Rates from Quantitative Textural Data: Inversion of Crystal Size Distribution. *Journal of Petrology* **54**, 913–931.

Spillar, V. & Dolejs, D. (2015). Heterogeneous nucleation as the predominant mode of crystallization in natural magmas: numerical model and implications for crystal-melt interaction. *Contributions to Mineralogy and Petrology* **169**, 4–19.

Spohn, T., Hort, M. & Fischer, H. (1988). Numerical Simulation of the Crystallization of Multicomponent Melts in Thin Dikes or Sills. 1. The Liquidus Phase. *Journal of Geophysical Research* **93**, 4880–4894.

Toramaru, A. (2006). BND (bubble number density) decompression rate meter for explosive volcanic eruptions. *Journal of Volcanology and Geothermal Research* **154**, 303–316.

Toramaru, A., Noguchi, S., Oyoshihara, S., Tsune, A. (2008). MND(microlite number density) water exsolution rate meter. *Journal of Volcanology and Geothermal Research* **175**, 156–167.

Tsuchiyama, A. (1985). Dissolution kinetics of plagioclase in the melt of the system diopside-albite-anorthite, and origin of dusty plagioclase in andesites. *Contributions to Mineralogy and Petrology* **89,** 1–16.

Tsuchiyama, A. & Takahashi, E. (1983). Melting kinetics of a plagioclase feldspar. *Contributions to Mineralogy and Petrology* **84**, 345–354.

Tsune, A. & Toramaru A. (2007). A simple model of oscillatory zoning in magmatic plagioclase: Development of an isothermal undercooling model. *American Mineralogist* **92**, 1071–1079.

Underwood, E. (1970). *Quantitative stereology*. Addison Wesley-Longman, Reading, MA. 274 pp.

Ustunisik, G., Kilinc, A. & Nielsen, R. L. (2014). New insights into the processes controlling compositional zoning in plagioclase. *Lithos*, **200-201**, 80–93.

Vinet, N. & Higgins, M. D. (2010). Magma solidification processes beneath Kilauea Volcano, Hawaii: a quantitative textural and geochemical study of the 1969 – 1974 Mauna Ulu lavas. *Journal of Petrology* **51**, 1297–1332.

Vinet, N. & Higgins, M. D. (2011). What can crystal size distributions and olivine compositions tell us about magma solidification processes inside Kilauea Iki lava lake, Hawaii? *Journal of Volcanology and Geothermal Research* **208**, 136–162.

Wager, L. R. (1961). A note on the origin of ophitic texture in the chilled olivine gabbro of the Skaergaard intrusion. *Geological Magazine* **98**, 353–366.

Yoder, H. S. & Tilley, C. E. (1962). Origin of basalt magmas: an experimental study of natural and synthetic rock systems. *Journal of Petrology* **3**, 342–532.

Zellmer, G. F., Blake, S., Vance, D., Hawkesworth, C. & Turner, S. (1999). Short plagioclase residence times at two island arc volcanoes (Kameni islands, Santorini, and Soufriere, St. Vincent) determined by Sr diffusion systematics. *Contributions to Mineralogy and Petrology* **136**, 345-357.

Zieg, M. J. & Lofgren, G. E. (2006). An experimental investigation of texture evolution during continuous cooling. *Journal of Volcanology and Geothermal Research* **154**, 74–88.

Zieg, M. J. & Marsh, B. D. (2002). Crystal Size Distributions and Scaling Laws in the Quantification of Igneous Textures. *Journal of Petrology* **43**, 85–101.